Eur. Phys. J. A **8**, 331–354 (2000)

THE EUROPEAN PHYSICAL JOURNAL A

Yields of products from fast neutron-induced fission of ^{233}U measured by means of an Isotope Separator On-Line (ISOL) system

J. Galy[1,2,3], B. Fogelberg[1], F. Storrer[2], and H. Mach[1]

[1] Department of Neutron Research, Uppsala University, S-61182 Nyköping, Sweden
[2] CEA, CEN Cadarache, DER/DRN/SPRC/LEPh Bât 230, F-13108 S_t Paul lez Durance, France
[3] Now at the Institute for Trans Uranium Elements, European Commission, Postfach 2340, D-76125Karlsruhe, Germany

Received: 19 April 2000
Communicated by J. Äystö

Abstract. A comprehensive study has been carried out of the yield pattern of fission products formed in fast neutron-induced fission of ^{233}U. The isotope separator on-line facility at Studsvik to the R2-0 nuclear reactor was used for rapid separation of the fission products. At a target temperature of 2250 °C fission products of the elements from zinc ($Z = 30$) to barium ($Z = 56$) are released, with the exception of yttrium, zirconium, niobium, molybdenum, technetium, ruthenium and rhodium. The individual isotopes are then available for study, implying that an almost complete mapping of the yield distribution can be made. In the analysis, the delay between production and measurement and the overall separator efficiency for three consecutive elements (the one under study and its parent and grand parent) are taken into account. Independent and/or cumulative yields have been obtained for 203 nuclear species, among them 59 isomeric states.

PACS. 25.85.Ec Neutron-induced fission – 23.20.Lv Gamma transitions and level energies

1 Introduction

Nuclear fission is a dynamical process, and so is the evolution of the fission yield pattern in the early stages following the fission reaction. The over-all mass chain distribution does not change with time, if the small effect due to the delayed neutrons is neglected. The delayed neutron effect is highly important, however, for the most neutron rich fission products undergoing rapid sequences of short-lived β-decays. A good knowledge of the total independent yield pattern, including such short-lived products, is needed for the development and testing of models of the nuclear fission. Such a knowledge can also give hints regarding the dynamics of the fission process. Measurements of the independent yields are thus of substantial interest, but pose difficulties because time is an important factor, requiring advanced measurement technology. The experimental difficulties are the reason that only a small fraction of the yields, independent and/or cumulative, of the about 900 primary products have been measured for any fission reaction. About 25% of the product yields have been measured, at the best, for the fissioning system of technical importance and usually about 1% or less for other fission reactions involving readily available long-lived nuclides.

In the present work, a comprehensive study of the yield pattern of fission products formed in the fast fission of ^{233}U is presented. The study was done using the isotope separator on-line facility OSIRIS at Studsvik [1,2]. Using the technique developed by Rudstam and collaborators [2], a large fraction of the independent yield distribution in the fast fission of ^{233}U has been measured, including many isomers and some nuclides belonging to the region of "symmetric" fission, where the two fragments have nearly equal masses. Although the number of symmetric fission events is very small, the data obtained in this region are of strong theoretical and diagnostic interest. The information both on the distribution of independent yields among different isomeric states and the charge distribution in the region of symmetry is scarce so far, as these values are practically inaccessible to most of the other experimental techniques. It is in practice only the ISOL method, including the IGISOL concept [3], that gives access to data on the yields of short-lived isomers. Almost all the yields obtained presently are new data since *no experimental independent yields* in the fast fission of ^{233}U were available prior to this study. Using an isotope separator presents as well some shortcomings: because the number of fissions in the target is not directly measurable, normalization using external experimental data is required. If there were no experimentally determined normalization data, then one would have to use estimated values increasing the uncertainty on the resulting yields. The present studies, based

on γ-assay, have shown that there is a strong need for precise data on γ-ray intensities to improve the accuracy of the results obtained with the OSIRIS method. Furthermore, the yield determination is based on the knowledge of the delay parameter and ionization efficiency of each chemical species released from the target. A careful study of these parameters is required in order to understand better the release and the ionization mechanisms of the fission products from the integrated target ion-source and to further improve the capability of this technique to measure the fission yield data.

We summarize here all the results from the yield measurements of ^{233}U(n_f, f) including also instrument related studies of the temperature dependence of the delay parameter and overall efficiency of the isotope separator.

The current investigations of Accelerator Driven Systems (ADS) [4–6] for the purposes of both energy production and waste reduction are an obvious additional motivation to improve the fission yield data for the ^{232}Th/^{233}U fuel cycle. The Th cycle offers some advantages (larger fuel reserves, less transuranic waste, less risk for proliferation) but requires a substantial technology development. An improved quality of the pertinent basic nuclear data is also required, where the present work can be seen as a first step regarding the detailed fission properties.

2 Design and characterization of a filtered fast neutron spectrum

The thermal neutron fission cross-section of ^{233}U is larger by a factor of about 200 than the at MeV energies. As the R2-0 reactor, used as a neutron source in the present studies, is a water-moderated research reactor, it was necessary to investigate whether the neutron spectrum at the target irradiation position could be sufficiently filtered to give predominantly fast fission events in the ^{233}U target. A theoretical study [7] to find the optimal filtering was conducted using two different transport calculations. A deterministic computation with the DORT code [8] was performed to predict the shape of the spectrum using different materials and different geometries of the neutron filter. (The DORT code uses 26 energy groups from 0.03 eV to 20 MeV to describe the neutron spectrum.) A filter material of B_4C with a thickness of 2 cm was found optimal to cut off both thermal and epithermal neutron components of the flux. A probabilistic method (MCNP^{TM} [9] was also employed to verify the deterministic calculations. The spectral shapes calculated at the target position with and without a boron filter are shown in fig. 1, illustrating an effective filtering out of the neutron flux for neutron energies lower than 1 keV. The most relevant parameter for our purposes is the fraction of fission events induced by fast neutrons. The ratio of the fast to the total fission rate, $(\sum_f \cdot \Phi_{fast})/(\sum_f \cdot \Phi_{total})$, found with the help of both methods is summarized in table 1, showing that up to 99% of the fission events are due to fast fission of ^{233}U, depending somewhat on the low-energy cut-off used to define the concept of "fast neutrons". The DORT and MCNP calculations gave, respectively, the following average neutron energy in the spectrum: $\langle E_n \rangle_{DORT} = 1.19$ MeV and $\langle E_n \rangle_{MCNP} = 1.25$ MeV with a maximum flux of 1.7×10^{11} n/cm^2/s.

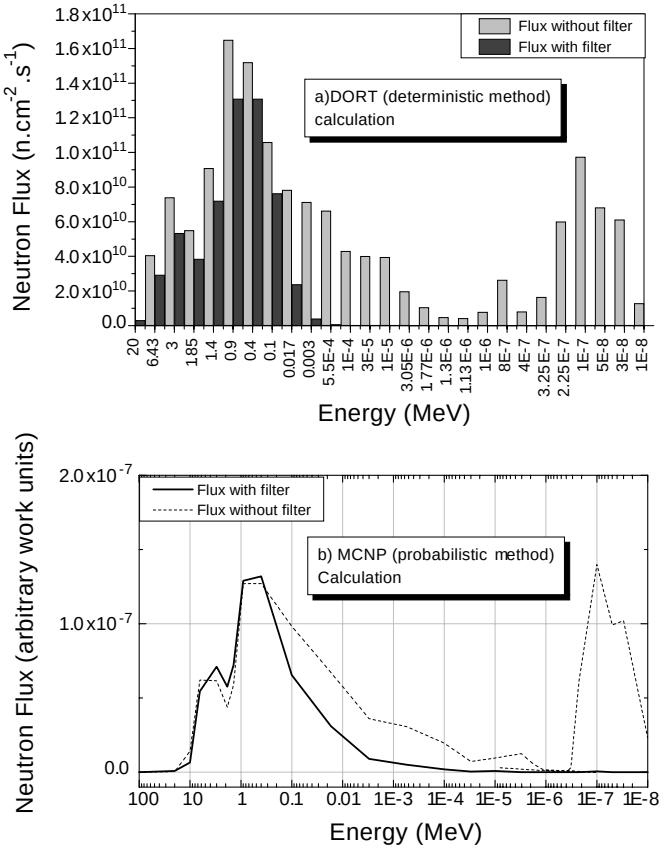

Fig. 1. a) Flux calculated at the target position with the deterministic code DORT, with and without the B_4C filter shielding the ^{233}U target. b) Same calculations as in a) but with the probabilistic MCNP code.

Table 1. Comparison of the results obtained with DORT (deterministic method) and MCNP (probabilistic method) for the $(\sum_f \cdot \Phi)_{fast}/(\sum_f \cdot \Phi)_{total}$ ratio.

	DORT Calculation	MCNP Calculation
No Filter	$8.2 \cdot 10^{-3}$	$1.5 \cdot 10^{-3}$
Filter: $E_{nfast} > 100$ eV	0.99	0.99
Filter: $E_{nfast} > 3$ keV	0.80	0.95
Filter: $E_{nfast} > 100$ keV	0.70	0.78

Experimental irradiations of different (thermal, resonance and threshold) activation foils, with and without a B_4C filter, were performed to simulate the conditions of the ^{233}U target, and gave a good agreement between the measured and calculated spectra.

The filter employed during the fission yield measurements was made in a "top hat" configuration consistent with that used in the calculations. The filter enclosed the ion source and the associated high voltage insulator, with

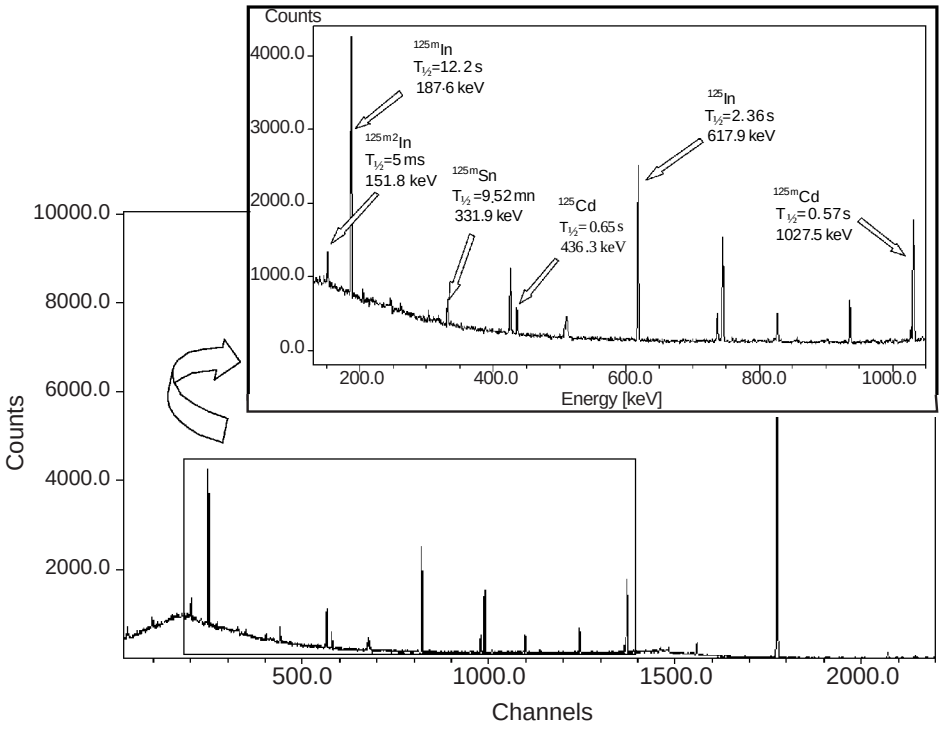

Fig. 2. Gamma-ray assay of on-line separated sample of fission products for the mass 125.

a wide "brim" to prevent back scattering of neutrons into the inner volume of the filter.

3 Experimental techniques

The mass separated beams of fission products obtained using the OSIRIS facility generally contain contributions from a few different isobars. The different isobars can be identified by following the growth and decay of their radiations using a multi spectrum scaling (MSS) technique. In the case of the fission yield measurements, the MSS cycle was chosen to consist of four time groups: a background group followed by a beam collection (=growth) time divided into three equal time groups. The ion beam was collected on a moveable Al-coated plastic tape in front of the spectrometry system. After a MSS cycle, the tape was moved to position the old sample in a shielded location, and a new cycle was initiated. The measurement cycles were repeated until data of sufficient quality had been obtained. It was often necessary to take data with different MSS group times on the same isobaric chain in order to enhance specific components.

The spectrometry system consisted of two Ge spectrometers (of 50% and 80% relative efficiency) and a plastic scintillator for monitoring the total β-particle counting rate. The Ge spectrometers were well shielded from the room background with bricks of Fe, Pb and borated paraffin, and were shielded from β-particles by discs of plastic. As discussed later, a relative calibration of the detector system is quite sufficient for the present purposes. We used sources of ^{152}Eu and ^{90}Rb (the latter obtained on-line) for the construction of relative efficiency curves up to an energy of about 3.5 MeV. The data acquisition was made using an ADC range of 4 k channels, into three 16 k channel memories, each divided into four sections to accommodate the four MSS groups. Clock pulses from a pair of pulse generators were fed to the pre-amplifiers of the Ge spectrometers for monitoring the dead time in each individual spectrum. It was important to fine-tune the counting rate of the Ge spectrometers in order to obtain a desirable precision in a short time without saturating the spectrometry system. In general, the counting rate was adjusted by simply modifying the power level, and hence the neutron flux of the R2-0 reactor, but some adjustment was also possible through the selection of the MSS group times.

The quality of the ion beam from the mass separator can be influenced by a number of factors, some of which are difficult to keep constant during long periods of time. We selected (somewhat arbitrarily) the $A = 97$ isobars to serve as a reference for the beam quality, and interspersed the yield measurements with frequent control measurements at $A = 97$, subsequently used to correct the data for variations in the beam intensity.

The abundance of the various isobaric components in the samples was determined from identified γ-ray peaks in the spectra, as shown in fig. 2. The uncertainty of the results therefore depends largely on the branching ratios of the γ-rays chosen for the conversion of peak areas into number of atoms. In several cases the absolute value of these branching ratios is not very accurately known, giving large errors of the yields. In some cases it was possible to derive new and improved values of the branching ra-

tios by combining the observed isobaric abundancy data with the information on the total β-counts in the plastic scintillator. Generally, several γ-rays were used for each nuclide. This improves the statistics and reveals handling errors such as contaminated γ-peaks or mistakes in the input of data for the computer calculations.

The on-line technique for the fission yield measurements has the advantage of being sensitive (yield values down to about 10^{-4}% can be determined in fast fission) and fast enough so very short-lived products (*e.g.* ^{125m2}In with a half-life $T_{1/2} = 5\,\mathrm{ms}$) near the "symmetric" region of the mass distribution can also be observed. As mentioned before, the elements from Y ($Z = 39$) to Rh ($Z = 45$) cannot, however be obtained via this method. Furthermore, the separation efficiency for the lanthanides was too low to allow efficient measurements during the fast fission of ^{233}U. Within these restrictions, about 200 independent yields were measured including some isomeric yields, covering the mass range from 74 to 147 and the charge range from 29 (Cu) to 56 (Ba). This range of nuclides represents a very large amount of spectra to be analyzed (about 1200).

The present experiments depended on the use of a rare and irreplaceable target of about 0.25 g of ^{233}U. This target was operated at a slightly lower temperature than normally used (2250 °C instead of 2350 °C), in order to reduce the probability of an accidental breakdown during the approximately 3 weeks of beam time needed for the spectroscopic studies and the control measurements. As a consequence, the production of the lanthanide nuclides became too low for practical measurements as mentioned above. (On the other hand, the nuclear data in this region is in general too poorly known for analytical purposes such as yield determinations.) The second region of "missing nuclides", from Y to Rh, can for ISOL purposes be produced only by means such as the He-jet technique, which is virtually impossible to implement in the geometry of a reactor channel.

4 Analysis of the data

4.1 Experimental considerations in the yield derivation

An analysis of all gamma-ray spectra with regard to the most characteristic lines due to all nuclides expected to be present, was the first step in the yield derivation. This "raw" nuclide abundance data had subsequently to be corrected for experimental effects such as beam intensity fluctuations, which were monitored by frequent control measurements, and pulse pile-up losses, which were determined from pulser clock peaks in the spectra. The fact that the measurements were divided into MSS time groups permitted identification of specific half-life components and made it possible to identify contaminated peaks. Other important corrections are due to the decay losses caused by the finite delay between a fission event and the separation/collection of a specific nuclide, as well as the fact that different chemical elements are separated with different efficiencies. A detailed analysis of the method for such corrections has been given by Rudstam [2]. A summary of the aspects of importance for the present work is given below, together with a short account of the normalization process that is needed.

The computer program [2] written for the analysis of the measurements calculates independent and cumulative yields of a specified isotope, taking into account the contributions from both grandparents and parents (via β-decays and delayed neutron emission) to the observed number of decays of the daughter. The analysis thus requires the knowledge of the delay properties of three consecutive elements, the one being studied, and its parent and grandparent. The origin of the delay is instrumental in nature.

The high temperature ion-source [10] of OSIRIS includes the target of fissile material in the shape of a porous graphite cylinder impregnated with uranium. The ion-source can be run with a target temperature up to 2500 °C. In the present experiments, a lower temperature of 2250 °C was chosen for the safety of the target, since only a limited amount of ^{233}U was available. The atoms of different element escape from the target either entirely by diffusion (through the target material) or by a combination of diffusion and desorption from the surface of the target. These two processes are the time controlling steps of the release mechanism, and need to be treated differently in the analysis of the delay time in the target. Fortunately, it has been shown by Rudstam [11] that the final result is not very sensitive to the exact nature of the release mechanism if the delay is short, and that both processes give very similar results. In the present analysis, desorption controlled release is assumed for all the elements of interest except for the two noble gases (xenon and krypton), for which no hold-up at the surface is expected, they are thus assumed to be released by diffusion only.

Whether the time controlling step is diffusion or desorption, one can still observe significant differences between the release times of the atoms of different elements. The process of the release can to a good approximation be described using only the two parameters μ (the delay parameter) and the ionization efficiency η (in practice the total efficiency given by the ratio of the numbers of atoms collected to those formed in fission). These parameters need thus to be determined experimentally for each chemical species of interest.

In the previous yield determinations at OSIRIS, the two-point normalization method [11,12] was used to determine these parameters. This approach requires known yields, Y_n, of two isotopes of the same element, one with a long and the other with a short half life in comparison to the delay in the isotope separator system, implying that the value of the delay constant falls in between their decay constants. The ratio $\eta R/Y_\mathrm{n}$, with R being the nuclide production rate is then plotted *versus* μ for both isotopes. More explicitly, the ratio is

$$\frac{\eta R}{Y} = \eta N \varphi \sigma_\mathrm{fiss}, \tag{1}$$

where the number of target atoms, the particle flux, and the formation cross-section are given in obvious notation.

The ratio will vary with μ, but there is only one value of μ which satisfies both normalization points. The corresponding value of the ratio is then proportional to the total separator efficiency, which can be determined on an absolute scale if appropriate values of the cross-section etc. are entered.

In the case of ^{233}U(n$_f$, f), it is not possible to find suitable normalization points since very few yields are known experimentally. In order to circumvent this difficulty another approach was applied, drawing on the experience obtained in the previous studies, and during performance tests of targets and ion sources. The performance tests show that the release time, and hence the delay parameter depends on the concentration of uranium in the porous graphite of the target and also on the temperature. There is no observed significant difference between the delay properties of targets having essentially the same U/C ratio. It is thus a good approximation to use similar values of the delay parameters for the different elements as was found in the previous fission yield studies of ^{235}U, ^{233}U, and ^{238}U, see refs. [11], [12] and [13], respectively. However, these previous investigations were performed at a target temperature of 2350 °C, while the present data were taken at 2250 °C. It was therefore necessary to investigate the temperature dependence of the release of the fission products. This investigation can be performed by comparing the production yields of the mass-separator for a long-lived and a short-lived isotope of the same chemical species at different target temperatures. The long-lived isotope can be presumed not to suffer significant losses due to the delay in the target. Hence, any variation in the relative production yield of the short lived isotope is due only to the delay, and is a direct measure of the parameter F_{corr} employed in the analysis of delay losses [2] by Rudstam. This parameter, representing the inverse of the number of atoms surviving the decay losses, depends only on the delay parameter and the decay constant of interest and can be deduced from observed data once a value for the delay parameter is known for one isotope of a given element.

The decay losses in the production yields were studied in a special series of measurements at three different temperatures, 2150 °C, 2250 °C and 2350 °C, for most of the elements obtained as fission products. The production yields were deduced from peak areas in the γ-ray spectra in a similar way as in the main experiments. Losses in the yields due to temperature-dependent variations in the delay parameters were deduced by comparing measurements on nuclides with very different half lives, either on two isotopes of the same element, or by comparing the yield of a short-lived isotope with a long-lived species (such as a well-known daughter product) in the same sample. Subsequently, a weighted average of the delay parameters at 2350 °C was deduced from the previous experiments and corrected to apply at 2250 °C, which is the temperature of interest for the present work. The correction factors were found to be in the range from 1.0 to 1.5.

Also the efficiency of the ion source is influenced by different operating conditions. A lower temperature is obtained by a lower bombardment current, which latter is responsible for the ionization by electron impact. For most elements, the efficiency will thus be proportional to the bombardment current, which is reduced by about 25% when going from 2350 °C to 2250 °C. Some exceptions exist as discussed below.

The elements Rb, Cs have extremely low ionization potentials, and are almost completely thermally ionized already at 2000 degrees. There is no change in efficiency for these elements.

The elements Br, Kr and Xe have ionization potentials, which are higher than that of carbon. A higher temperature gives a higher concentration of carbon vapor, which leads to a loss of ionization for Br, Kr and Xe, due to charge exchange collisions with carbon atoms. In the range 2250 to 2350 °C, there is a balance between this loss and the increasing ionization due to the bombardment current. Thus, there is no temperature dependent change in efficiency in this temperature interval.

The modifications mentioned above, applied to previously determined values for the efficiency, have been used as a reasonable approximation in the calculations of the parent effects on the derived yields. A summary of previous and present values for delay and efficiency is given in table 2.

4.2 Special note for the case of Ge, As, and Se

Rudstam's method [11,12] for a simultaneous determination of the separator efficiency and the delay parameter is based on using the observed counting rates for two isotopes of the same element, having known yields and having quite different half lives. For the further analysis, the delay parameter is the most important item. The efficiency has little influence on the final yield values, since these are anyway normalized on some known value for each element.

The two-point method of Rudstam may lead to interdependent errors in the delay and efficiency, if erroneous data is being used in the analysis. An incorrect value for the gamma-ray branching gives an over- or underestimate of the number of atoms actually collected. A problem of this type has probably occurred in the analysis [11] of data for Ge, As and Se. The following nuclides were used:

^{80}Ge (24.5 s) and ^{83}Ge (1.9 s). The γ-ray branchings of both nuclides were deduced from the decay schemes. No measured data exists. The independent yield of ^{80}Ge is much smaller than the cumulative, giving a large uncertainty in this normalization point.

^{81}As (33 s) and ^{84}As (5.5 s). The γ-ray branching value of ^{81}As used by Rudstam (for the yields of ^{235}U) is a factor of two lower than the value obtained in a later experiment. Also ^{81}As has a small independent yield compared to the cumulative.

^{84}Se (195 s) and ^{88}Se (1.8 s). The γ-ray branching of ^{88}Se is uncertain by about a factor of two. Only one determination has been made, in a chemical separation experiment giving all Se isotopes simultaneously.

The analysis by Rudstam gives the efficiency for As to be 15–30 times higher than for Ge and Se. No such strong

Table 2. Delay parameter and separation efficiency used in the analysis. The data in the first two columns refer to the present work. Values from previous yield determinations are given in the subsequent columns. μ = Delay parameter, η = efficiency (number of atoms collected/number of atoms formed). η_R= ratio between η-parent and η-daughter, X_{233}= parameter used for $^{233}U(n_{th},f)$ analysis [11], X_{238} = parameter used for $^{238}U(n_f,f)$ analysis [12], X_{235} = parameter used for $^{235}U(n_{th},f)$ analysis [10]. μ and η_R are given at the target-ion source temperature $T = 2250\,^{\circ}C$ for the $^{233}U(n_f,f)$ analysis but at $T = 2350\,^{\circ}C$ for the previous values ($\mu_{233,238,235}$ and $\eta_{R,233,238,235}$).

Element	$\mu(s^{-1})$ Present work	$\eta_R(s^{-1})$ Present work	$\mu_{233}(s^{-1})$	$\eta_{R,233}$	$\mu_{238}(s^{-1})$	$\eta_{R,238}$	$\mu_{238}(s^{-1})$	$\eta_{R,235}$
Zinc	0.27 ± 15	1.000	0.39^{+77}_{-21}	1.000	0.22^{+13}_{-13}	1.000	0.26^{+10}_{+30}	1.000
Gallium	0.37 ± 15	0.48 ± 21	0.39^{+64}_{-19}	0.48 ± 21	0.6^{+22}_{-4}	0.43 ± 11	0.25^{+15}_{-9}	0.074 ± 13
Germanium	0.09 ± 3	2.7 ± 8	0.059^{+39}_{-29}	2.7 ± 8	0.22^{+21}_{-12}	6.2 ± 16	0.140^{+33}_{-26}	23 ± 3
Arsenic	0.0023 ± 7	1.000	0.00020^{+5}_{-4}	0.036 ± 5	0.00009^{+2}_{-2}	0.0052 ± 13	0.0019^{+4}_{-4}	0.070 ± 11
Selenium	0.0053 ± 10	1.000	0.0060^{+34}_{-2}	62 ± 11	0.0080^{+9}_{-8}	260 ± 50	0.0113^{+22}_{-22}	32 ± 5
Bromine	0.76 ± 35	0.71 ± 14	0.127^{+62}_{-38}	0.95 ± 18	0.49^{+41}_{-19}	0.47 ± 7	$4^{+\infty}_{-2}$	0.52 ± 5
Krypton	0.53 ± 25	1.35 ± 22	0.046^{+31}_{-20}	1.35 ± 22	0.67^{+44}_{-22}	0.98 ± 15	0.67^{+66}_{-27}	1.72 ± 20
Rubidium	1.10 ± 30	0.0092 ± 17	2.51^{+96}_{-63}	0.0092 ± 17	1.06^{+20}_{-16}	0.0068 ± 7	0.45^{+14}_{-11}	0.00138 ± 30
Strontium	0.10 ± 5	4.00 ± 84	0.094^{+21}_{-17}	3.00 ± 63	0.26^{+3}_{-3}	17.0 ± 23	0.098^{+21}_{-17}	2.8 ± 7
Palladium	0.007 ± 4	1.000	0.0093^{+98}_{-54}	1.000				
Silver	1.07 ± 50	1.01 ± 41	0.41^{+500}_{-24}	1.01 ± 41	1.5^{+53}_{-11}	1.000	1.7^{+56}_{-11}	1.3 ± 5
Cadmium	0.29 ± 15	0.60 ± 28			0.40^{+81}_{-27}	0.61 ± 28	0.45^{+270}_{-27}	0.60 ± 28
Indium	0.31 ± 14	0.34 ± 13			0.34^{+25}_{-14}	0.34 ± 13	0.57^{+51}_{-25}	0.109 ± 4
Tin	0.76 ± 35	0.12 ± 5	0.0025^{+32}_{-17}	0.12 ± 5	$0.77^{+\infty}_{-53}$	1.97 ± 34	$2^{+\infty}_{-17}$	6.2 ± 16
Antimony	0.022 ± 11	2.00 ± 49	0.025^{+7}_{-5}	2.00 ± 49	0.034^{+20}_{-12}	0.95 ± 12	0.046^{+28}_{-16}	1.09 ± 24
Tellurium	0.020 ± 6	0.51 ± 11	0.025^{+6}_{-5}	0.51 ± 11	0.029^{+7}_{-6}	1.30 ± 17	0.035^{+14}_{-9}	1.26 ± 24
Iodine	0.33 ± 20	1.48 ± 19	0.045^{+18}_{-13}	1.48 ± 19	0.21^{+8}_{-5}	0.94 ± 12	$2^{+\infty}_{-1}$	1.23 ± 29
Xenon	0.044 ± 30	0.63 ± 31	0.12^{+12}_{-5}	0.84 ± 19	0.081^{+20}_{-16}	1.99 ± 26	0.045^{+41}_{-19}	3.3 ± 8
Cesium	0.69 ± 20	0.0173 ± 41	0.022^{+12}_{-7}	0.0173 ± 41	0.77^{+11}_{-9}	0.0154 ± 11	0.61^{+16}_{-11}	0.0042 ± 9
Barium	0.11 ± 6	6.13 ± 126	0.00899^{+33}_{-2}	4.60 ± 95	0.11^{+11}_{-6}	10.1(13)	0.14^{+18}_{-9}	5.0 ± 11

effect has been seen in the many measurements performed on the isobars with $A = 80$–85. The elements Ge, As and Se are chemically equivalent with Sn, Sb and Te. They have similarly high vapor pressures at the temperature of the OSIRIS target, and quite comparable ionization potentials. The separation efficiencies should therefore be comparable for these two sets of elements.

The efficiency can become quite low for elements with a very small vapour pressure. This is the reason why the elements with $Z = 40$–45 are not seen at OSIRIS. For more volatile elements, the efficiency is mainly related to the magnitude of the ionization potential.

If this potential is less than about 7 eV, a component of surface ionization has a strong influence. The completely dominant ionization mechanism for elements with higher potentials is the electron impact ionization. The incident electrons have a wide energy spread from low energies up to about 150 eV, resulting in a rather uniform probability for ionization for all elements, except for some dependence on the absolute magnitude of the ionization potential. There is no plausible (or even conceivable) mechanism that can cause the high ionization efficiency reported by Rudstam for the element As (see also fig. 3). The fact that a very low efficiency is obtained for Se, is probably due to an incorrect parent effect, which has been influenced by the high efficiency used for As in the data analysis.

The most probable scenario is that Ge, As and Se are obtained with nearly the same efficiencies, and that the delay of As in the target is considerably smaller than given by Rudstam [11].

5 Resulting yields in the fast neutron fission of ^{233}U

The fission yields obtained using OSIRIS are relative values proportional both to the independent and the cumulative formation over a range of isotopes. These relative values need to be normalized. The normalization is done by comparing the yield value $N\Phi\eta\sigma Y$, where Y is the yield in percent, with the known yield of a given isotope. This gives a value of $N\Phi\eta\sigma$. For a given experiment this is a constant ($= C_{TZ}$), which can be used for the determination of the yield of all other isotopes of the same element by the relation (Yield Value/C_{TZ}).

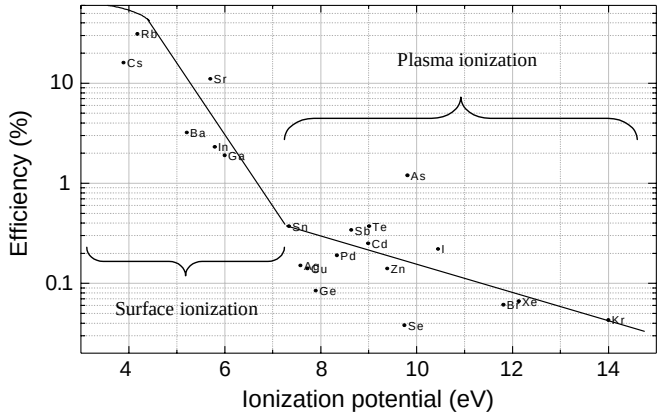

Fig. 3. Total separation efficiencies at OSIRIS as measured by Rudstam. The data for lanthanides are not included. The uncertainties are of order of ±50% in most cases, and can be substantially larger in cases where γ-ray branching data are poorly known. The given efficiencies for Se and As are unphysical and should not be trusted. The efficiencies for these elements are expected to be near 0.25 in both cases.

The lack of experimental data for the ^{233}U(n$_f$, f) reaction has motivated a campaign of off-line measurements [15] in order to get some normalization points for the determination of the C_{TZ} factor. This set of measurements led to the determination of more than 50 cumulative yields of nuclei, with half-lives ranging from 10 min to 15 days. A number of these values were found to be suitable normalization points for some specific elements. In other cases, where experimental data were unavailable, the recommended values from the Z_p-model of Wahl [15–18] or the calculated values from the non-equilibrium thermodynamic model of Grashin *et al.* [19] were used for the normalization. Table 3 gives a summary of the normalization procedure for each element, and the resulting yields are given in tables 4–23. These tables also include a comparison with yield values calculated from the Z_p-model of Wahl [15–18] and from the non-equilibrium thermodynamic model of Grashin *et al.* [19]. The latter model includes a method for the partition of the yields on different isomeric states. In the case of the Z_p-model, we used the semi-empirical approach of Rudstam [20] for the partition on isomers.

The main nuclear data used in the analysis are summarized in ref. [21], and is also available on request from the authors. Most of the branching ratios as well as the decay data are taken from a survey made by Rudstam [22] and from the Table of Isotopes [23].

5.1 Copper isotopes

The present experiment was not aiming at yield determinations of the Cu isotopes, partly because there is no previous information about the delay properties and the separation efficiency of this element. One may assume that Cu should behave rather similarly to the chemical homologue Ag. Under this assumption, the observed intensity of the nuclide ^{74}Cu corresponds to a yield of about 10^{-4}%. This value has a high uncertainty and is not tabulated. No search for other Cu isotopes was performed.

5.2 Zinc isotopes

Zn is the lightest element studied systematically, and it has not been possible to correct for parent contributions. The parent effects have thus been neglected, and all Zn yields are regarded as cumulative, which is a good approximation.

The normalization was made on ^{76}Zn using the Z_p-model, which has a high uncertainty here due to the lack of experimental data. As a result, large uncertainties on the measured yields at OSIRIS are obtained. Within the errors, the evaluated/calculated values agree with our measured data.

5.3 Gallium isotopes

Since no experimental normalization data were available for Ga, the Z_p-model values for ^{80}Ga were used to derive C_{TZ}. Here again, the uncertainty on the normalization is high leading to a large uncertainty on the results.

The experimental yields and Wahl's recommended values agree reasonably well over the range of isotopes. One can notice that the calculations of Grashin *et al.* give lower values.

5.4 Germanium isotopes

The ^{82}Ge yield value from the Z_p-model used for normalization. The branching for ^{80}Ge remains uncertain, as mentioned in section 4.2, and the yield becomes a factor two lower if the branching from ref. [22] is used.

5.5 Arsenic isotopes

Arsenic is released rather slowly from the target. The isomer ^{82m}As has been used for normalization within the Z_p-model.

An unexpected high yield of ^{82g}As was noticed (10 times higher than the predicted value). A similar behavior has been observed in the thermal values by Rudstam [24], which leads to the assumption that the accepted γ-branching values from literature [23] must be re-viewed for this nuclide. Indeed, it was found by inspecting the data of the β-counter in our experiment that the branching values of the ^{82}As ground state are a factor of (5 ± 2) higher than given in [23] if the branching of the isomer is correctly given. The total number of observed β-counts is simply too low to allow for the very large ground state feeding in the accepted [23] decay scheme. The yield given in table 7 is based on the corrected branching value.

Table 3. Normalization of the experimental yields.

Normalization point[a]	Values used		Reference	Derived C_{TZ}[a]
	Y_{ind}	Y_{cum}		
^{76}Zn	$(7.65 \pm 5.89) \cdot 10^{-6}$	$(7.72 \pm 5.40) \cdot 10^{-6}$	[b]	0.0077 ± 0.0062
^{80}Ga	$(8.70 \pm 8.44) \cdot 10^{-5}$	$(8.75 \pm 8.40) \cdot 10^{-5}$	[b]	0.018 ± 0.017
^{82}Ge	$(1.10 \pm 0.75) \cdot 10^{-3}$	$(1.10 \pm 0.75) \cdot 10^{-3}$	[b]	0.0081 ± 0.057
^{82m}As	$(2.02 \pm 1.21) \cdot 10^{-3}$	$(2.02 \pm 1.21) \cdot 10^{-3}$	[b]	0.214 ± 0.152
^{84}Se	$(1.39 \pm 0.35) \cdot 10^{-2}$	$(1.67 \pm 0.37) \cdot 10^{-2}$	[b]	0.013 ± 0.004
^{87}Br		$(2.31 \pm 0.19) \cdot 10^{-2}$	[c]	0.223 ± 0.069
^{88}Kr		$(5.11 \pm 0.80) \cdot 10^{-2}$	[d]	4.01 ± 0.87
^{90}Rb		$(5.82 \pm 0.91) \cdot 10^{-2}$	[d]	2.65 ± 0.73
^{97}Sr		$(0.55 \pm 0.02) \cdot 10^{-2}$	[e]	0.122 ± 0.024
^{116}Pd	$(1.39 \pm 1.20) \cdot 10^{-4}$	$(2.33 \pm 1.25) \cdot 10^{-4}$	[b]	0.00031 ± 0.00022
^{119}Ag	$(1.38 \pm 0.84) \cdot 10^{-4}$	$(1.38 \pm 0.84) \cdot 10^{-4}$	[b]	0.014 ± 0.0083
^{124}Cd	$(1.13 \pm 0.75) \cdot 10^{-4}$		[f]	$(9.65 \pm 6.51) \cdot 10^{-3}$
^{128}In	$(1.40 \pm 0.40) \cdot 10^{-4}$		[f]	0.016 ± 0.008
^{129}Sn	$(1.47 \pm 0.58) \cdot 10^{-3}$		[f]	$(1.86 \pm 7.59) \cdot 10^{-3}$
^{130}Sb	$(9.70 \pm 4.66) \cdot 10^{-3}$	$(1.27 \pm 0.51) \cdot 10^{-2}$	[b]	$(7.62 \pm 1.84) \cdot 10^{-2}$
^{134}Te		$(4.68 \pm 1.06) \cdot 10^{-2}$	[d]	$(6.27 \pm 3.82) \cdot 10^{-2}$
^{135}I		$(4.96 \pm 0.73) \cdot 10^{-2}$	[d]	$5.06.10^{-1} \pm 9.33.10^{-2}$
^{135}Xe		$(5.47 \pm 0.88) \cdot 10^{-2}$	[d]	5.45 ± 1.19
^{140}Cs	$(3.36 \pm 0.66) \cdot 10^{-2}$	$(4.73 \pm 0.95) \cdot 10^{-2}$	[b]	$(6.16 \pm 2.27) \cdot 10^{-1}$
^{141}Ba		$(10.2 \pm 1.96) \cdot 10^{-2}$	[d]	0.013 ± 0.003

[a] See text, section 5, for details.

[b] Z_p-model [18].

[c] Experimental value [25].

[d] Off-line experiment [14].

[e] Experimental value [26].

[f] Thermodynamic model [19].

5.6 Selenium isotopes

The normalization of Selenium has been done using the Z_p-model value for the isotope ^{84}Se.

We can note that experimental data exist from the off-line measurements of cumulative yields [14], but the results turned out to be more accurate when normalizing on the independent yields.

The estimated and calculated values agree extremely well with the experimental results.

5.7 Bromine isotopes

For the normalization of Br, an experimental cumulative yield value [25] was used. The experimental yields of ^{84,85}Br are slightly higher than the estimated ones, but estimates and calculations agree well for the other measured values at OSIRIS.

5.8 Krypton isotopes

Experimental data from the off-line experiment [14] was used for normalization. The chosen normalization point was ^{88}Kr.

There is a general good agreement between the yields determined in this work and the calculated/estimated values.

5.9 Rubidium isotopes

The normalization point, ^{90}Rb has been chosen from data obtained in the off-line experiments [14]. Again, theory and calculations agree well with the experiment over this relatively large range of isotopes.

5.10 Strontium isotopes

Experimental data from ref. [26] has been used for normalization of Sr. The isotope ^{97}Sr was chosen as the normalization point. Experimental and estimated/calculated data agree.

5.11 Palladium isotopes

Ru and Rh do not seem to be released from the target at all, but decay to Pd isotopes in the target material, and no measurement can be done for these elements. In such a case, the cumulative yields of Pd are obtained in the analysis and the independent yields are tabulated as equal to these. Again, the Z_p-model had to be used for the normalization, which was done at ^{116}Pd.

Experimental and estimated/calculated data agree.

5.12 Silver isotopes

Again, no experimental yields have appeared in the literature, and we have to rely on an estimated value from the Z_p-model for ^{119}Ag.

The values from the Z_p-model and from the thermodynamical model of Grashin *et al.* agree well with the experimental data.

5.13 Cadmium isotopes

Here again, no experimental values could be found in the literature. Furthermore, Wahl's estimates are not reliable for these isotopes due to a very large uncertainty. We therefore normalize on a value for ^{124}Cd from Grashin's calculation [19].

As shown in the table, data taken from the Z_p-model estimates for the mass range 123–127 are hardly realistic, giving a spread of data over 4 orders of magnitude. One could note that a similar behavior was noticed also with the values from the thermal fission of ^{233}U measured by Rudstam [24]. A difference of 2 orders of magnitude was found between the yield values measured by Rudstam and the Z_p values for the thermal fission of ^{233}U.

The shape of the yield distribution calculated by Grashin [19] agrees rather well with experimental one.

5.14 Indium isotopes

Indium is another element for which no experimental data has appeared in the literature, and a calculated value from Grashin *et al.* [19], of the independent yield of ^{128}In, has been used for normalization. The values from the Z_p-model could not be used due to very large uncertainties.

In general, the In isotopes have isomers. Data were obtained for many of these, resulting in a total of 28 nuclidic yields for In. The predicted and calculated values show a generally good agreement with this large experimental data set.

5.15 Tin isotopes

The independent yield value of ^{129}Sn from Grashin's calculation [19] was used to normalize the measured data. Experimental and calculated/estimated data agree over the isotopic range. One may note the high uncertainties of the Z_p-model predictions. The long half-life of ^{126}Sn precluded an experimental determination for this nuclide.

5.16 Antimony isotopes

Both the independent and cumulative yield values of ^{130}Sb in the Z_p-model were used for the normalization. The experimental value for ^{131}Sb is somewhat higher than the model predictions, which otherwise show a good agreement with our data.

5.17 Tellurium isotopes

Experimental data for ^{134}Te from the off-line experiments [14] was used in the normalization. All calculated/predicted values agree within errors.

5.18 Iodine isotopes

A value from the off-line experiments [14] was used for the yield normalization on ^{135}I. The experimental yield values for ^{134}I and ^{140}I are slightly higher than expected from the models, which otherwise agree well with the experimental trend.

5.19 Xenon isotopes

For xenon, there is every reason to expect *diffusion*-controlled release, and this was assumed in the analysis. A cumulative yield value for ^{135}Xe from the off-line experiments [14] was used for normalization. Very good agreement is found between estimated/calculated values and our experimental data.

5.20 Cesium isotopes

No experimental yield data were available for these isotopes. Both the independent and the cumulative yield values of ^{140}Cs from the Z_p-model were used for normalization. The theoretical and estimated values agree well with the experimental data over a wide isotopic range and a very large span of yield values.

5.21 Barium isotopes

The off-line value obtained [14] for ^{141}Ba was chosen for normalization. Estimated and calculated data agree, here again, with the experimental ones.

6 Discussion

6.1 Cumulative yields

The cumulative yields reported in the present work are plotted *versus* mass number in fig. 4. For isotopes with two or three isomeric states (including the ground state) the yields given are the sum of cumulative isomeric yields. The points are joined by straight lines as a guide for the eye.

Table 4. Yields of zinc isotopes and comparison with systematics.

Isotope	Independent yield				Cumulative yield	
	Half-life	This work	Z_p-model	Grashin's model	This work	Z_p-model
	(s)	0.001%	0.001%	0.001%	0.001%	0.001%
^{74}Zn	95.6	2.39 ± 1.98	2.64 ± 2.88	2.64 ± 1.43	2.39 ± 1.98	2.78 ± 3.0
^{75}Zn	10.2	2.33 ± 1.86	5.21 ± 4.64	2.29 ± 1.16	2.33 ± 1.86	5.35 ± 4.66
^{76}Zn	5.6	7.65 ± 6.13	7.65 ± 5.89	1.77 ± 0.85	7.65 ± 6.13	7.72 ± 5.94
^{77m}Zn	1.05	0.23 ± 0.20			0.23 ± 0.20	
^{77}Zn	2.08	2.37 ± 1.93	4.61 ± 3.92	0.96 ± 041	2.37 ± 1.93	4.63 ± 3.93
^{78}Zn	1.47	2.37 ± 2.0	1.89 ± 2.67	0.49 ± 0.19	2.37 ± 2.0	1.90 ± 2.67

Table 5. Yields of gallium isotopes and comparison with systematics.

Isotope	Independent yield				Cumulative yield	
	Half-life	This work	Z_p-model	Grashin's model	This work	Z_p-model
	(s)	0.001%	0.001%	0.001%	0.001%	0.001%
^{74}Ga	487.2	2.36 ± 0.97	0.04 ± 0.14	2.55 ± 1.06	3.06 ± 2.97	2.83 ± 3.06
^{75}Ga	126	2.08 ± 2.01	6.86 ± 5.97	5.94 ± 2.60	4.14 ± 4.02	6.86 ± 5.97
^{76}Ga	29.8	3.76 ± 3.64	7.09 ± 5.17	8.39 ± 3.48	9.02 ± 8.75	14.8 ± 10.4
^{77}Ga	13.0	9.78 ± 9.49	21.2 ± 12.7	9.71 ± 3.82	13.1 ± 12.7	25.8 ± 15.0
^{78}Ga	5.09	26.0 ± 25.2	23.9 ± 12.7	8.53 ± 2.96	29.0 ± 28.2	25.8 ± 12.4
^{79}Ga	2.63	23.4 ± 22.7	22.3 ± 13.4	6.24 ± 1.92	23.4 ± 22.7	22.7 ± 13.4
^{80}Ga	1.66	8.70 ± 8.44	8.70 ± 8.44	3.20 ± 0.83	8.70 ± 8.44	8.75 ± 8.40
^{81}Ga	1.23	3.79 ± 3.68	2.93 ± 5.66	1.26 ± 0.32	3.79 ± 3.68	2.93 ± 5.66

Table 6. Yields of germanium isotopes and comparison with systematics.

Isotope	Independent yield				Cumulative yield	
	Half-life	This work	Z_p-model	Grashin's model	This work	Z_p-model
	(s)	0.001%	0.001%	0.001%	0.001%	0.001%
^{77m}Ge	52.9	1.72 ± 1.28	1.22 ± 1.77	1.83 ± 0.61	1.72 ± 1.28	1.22 ± 1.77
^{78}Ge	5280.0	24.0 ± 64.7	44.5 ± 23.6	43.2 ± 13.7	64.2 ± 60.4	70.4 ± 33.8
^{79m}Ge	39.0	55.9 ± 42.0	87.3 ± 75.1		57.8 ± 43.4	109 ± 75.5
^{79}Ge	18.9	48.0 ± 57.3	16.3 ± 14.0	68.5 ± 18.0	73.3 ± 63.3	207 ± 143
^{80}Ge	24.5	393 ± 295	185 ± 72.2	94.9 ± 20.9	7406 ± 305	194 ± 73.8
^{81m}Ge	7.5	42.0 ± 32.1	31.6 ± 27.8		44.1 ± 33.2	34.1 ± 28.3
^{81}Ge	7.6	133.0 ± 94.6	139 ± 122	79.1 ± 12.8	134 ± 95.1	139 ± 122
^{82}Ge	4.6	110.0 ± 76.9	110 ± 74.7	55.2 ± 10.8	110 ± 76.9	110 ± 74.9
^{83}Ge	1.9	7.96 ± 5.65	27.6 ± 36.1	13.0 ± 2.1	7.96 ± 5.65	27.6 ± 36.2

Table 7. Yields of arsenic isotopes and comparison with systematics.

Isotope	Independent yield				Cumulative yield	
	Half-life	This work	Z_p-model	Grashin's model	This work	Z_p-model
	(s)	0.1%	0.1%	0.1%	0.1%	0.1%
^{80}As	15.2	4.19 ± 1.75	0.63 ± 0.28	1.44 ± 0.26	4.45 ± 1.75	2.57 ± 0.90
^{81}As	33.3	4.86 ± 1.60	2.46 ± 0.84	2.78 ± 0.41	4.99 ± 1.62	4.20 ± 1.39
^{82}As	19.1	2.93 ± 0.91	1.86 ± 1.12		14.6 ± 4.58	2.97 ± 1.36
^{82m}As	13.6	1.90 ± 0.73	2.02 ± 1.21	3.34 ± 0.37	1.90 ± 7.32	2.02 ± 1.21
^{83}As	13.4	1.80 ± 0.93	4.40 ± 1.49	2.91 ± 0.44	1.78 ± 0.91	4.67 ± 1.54
^{84}As	4.0	1.61 ± 0.69	2.13 ± 1.041	1.14 ± 1.68	1.61 ± 0.69	2.18 ± 1.07

Table 8. Yields of selenium isotopes and comparison with systematics.

Isotope	Independent yield				Cumulative yield	
	Half-life	This work	Z_p-model	Grashin's model	This work	Z_p-model
	(s)	0.1%	0.1%	0.1%	0.1%	0.1%
^{83m}Se	70.1	2.94 ± 1.03	1.29 ± 0.81	1.81 ± 0.18	3.05 ± 1.07	4.56 ± 1.37
^{83}Se	1338	5.44 ± 1.71	5.68 ± 3.58	5.87 ± 0.87	5.50 ± 1.73	7.09 ± 1.91
^{84}Se	186	18.1 ± 6.61	13.9 ± 3.49	18.7 ± 2.84	18.4 ± 6.71	16.7 ± 3.9
^{85}Se	31.7	13.9 ± 4.91	15.7 ± 4.2	12.5 ± 2.08	13.9 ± 4.91	16.2 ± 4.2
^{86}Se	14	10.2 ± 3.63	13.6 ± 5.0	7.34 ± 1.65	10.2 ± 3.63	13.8 ± 5.1

Table 9. Yields of bromine isotopes and comparison with systematics.

Isotope	Independent yield				Cumulative yield	
	Half-life	This work	Z_p-model	Grashin's model	This work	Z_p-model
	(s)	0.1%	0.1%	0.1%	0.1%	0.1%
^{84m}Br	360	2.19 ± 0.79	0.91 ± 0.98	3.06 ± 0.45	2.19 ± 0.79	0.91 ± 0.98
^{84}Br	1908	7.65 ± 1.41	0.83 ± 0.91	1.45 ± 0.15	52.3 ± 18.8	17.5 ± 3.86
^{85}Br	174	28.2 ± 27.1	8.17 ± 2.70	14.9 ± 2.2	52.9 ± 25.8	24.3 ± 5.36
^{86}Br	55.1	27.8 ± 10.8	16.1 ± 3.9	20.2 ± 2.9	32.8 ± 12.3	26.9 ± 5.9
^{87}Br	55.6	23.1 ± 8.8	23.8 ± 5.5	17.0 ± 3.1	23.1 ± 8.8	28.8 ± 6.3
^{88}Br	16.4	10.3 ± 3.6	14.7 ± 4.3	8.65 ± 1.59	10.3 ± 3.6	16.0 ± 4.6
^{89}Br	4.4	8.37 ± 3.09	8.24 ± 3.96	3.66 ± 0.80	8.37 ± 3.09	8.40 ± 3.95

Table 10. Yields of krypton isotopes and comparison with systematics.

Isotope	Independent yield				Cumulative yield	
	Half-life	This work	Z_p-model	Grashin's model	This work	Z_p-model
	(s)	0.1%	0.1%	0.1%	0.1%	0.1%
^{85m}Kr	16128	0.62 ± 0.25	0.08 ± 0.23	0.13 ± 0.02	25.1 ± 4.7	24.4 ± 5.8
^{87}Kr	4578	49.0 ± 13.4	14.1 ± 5.4	11.4 ± 2.2	52.2 ± 14.0	43.2 ± 8.6
^{88}Kr	10224	51.0 ± 13.5	34.4 ± 8.6	34.7 ± 6.5	51.1 ± 13.5	50.5 ± 9.6
^{89}Kr	180900	46.4 ± 11.3	42.5 ± 8.5	39.5 ± 7.6	46.4 ± 11.3	50.2 ± 9.0
^{90}Kr	32.3	38.5 ± 9.1	42.3 ± 10.6	31.4 ± 7.9	38.5 ± 9.1	43.9 ± 10.5
^{91}Kr	8.6	10.4 ± 2.8	21.8 ± 8.1	11.4 ± 2.43	10.4 ± 2.8	22.2 ± 8.0
^{92}Kr	1.8	$B3.75 \pm 1.13$	8.52 ± 5.45	4.06 ± 1.00	3.75 ± 1.13	8.55 ± 5.47
^{93}Kr	1.3	1.29 ± 0.39	1.51 ± 1.84	0.86 ± 0.20	1.29 ± 0.39	1.51 ± 1.85

Table 11. Yields of rubidium isotopes and comparison with systematics.

Isotope	Independent yield				Cumulative yield	
	Half-life	This work	Z_p-model	Grashin's model	This work	Z_p-model
	(s)	0.1%	0.1%	0.1%	0.1%	0.1%
^{86m}Rb	61.0	0.11 ± 0.04			0.11 ± 0.04	
^{88}Rb	1066.8	2.50 ± 0.95	1.65 ± 1.49	3.33 ± 0.54	36.8 ± 14.0	52.2 ± 8.9
^{89}Rb	909.0	21.5 ± 7.6	8.58 ± 4.03	11.2 ± 1.9	24.9 ± 8.8	58.8 ± 10.0
^{90m}Rb	258.0	26.6 ± 10.4	12.5 ± 7.10	22.9 ± 4.0	26.6 ± 10.4	17.8 ± 7.1
^{90}Rb	158.0	14.2 ± 6.4	6.41 ± 3.65	4.72 ± 0.83	16.3 ± 7.1	45.7 ± 8.2
^{91}Rb	58.4	29.8 ± 11.1	36.8 ± 7.8	36.8 ± 7.2	30.3 ± 11.3	59.1 ± 11.2
^{92}Rb	4.5	36.0 ± 13.0	30.8 ± 6.8	22.2 ± 3.8	36.8 ± 13.3	39.4 ± 8.7
^{93}Rb	5.8	5.88 ± 2.01	21.2 ± 6.2	11.2 ± 2.3	5.95 ± 2.13	22.7 ± 6.6
^{94}Rb	2.7	4.42 ± 1.53	6.93 ± 3.33	4.30 ± 0.91	4.42 ± 1.53	7.14 ± 3.36
^{95}Rb	0.4	1.56 ± 0.50	2.42 ± 2.08	1.39 ± 0.30	1.56 ± 0.50	2.44 ± 2.07
^{96}Rb	0.2	0.31 ± 0.11	0.41 ± 0.66	0.29 ± 0.08	0.32 ± 0.12	0.41 ± 0.66
^{97}Rb	0.2	0.07 ± 0.02	0.06 ± 0.18	0.05 ± 0.02	0.07 ± 0.02	0.06 ± 0.18

Table 12. Yields of strontium isotopes and comparison with systematics.

Isotope	Independent yield				Cumulative yield	
	Half-life	This work	Z_p-model	Grashin's model	This work	Z_p-model
	(s)	0.1%	0.1%	0.1%	0.1%	0.1%
^{92}Sr	9792.0	20.2 ± 14.7	28.5 ± 9.7	21.6 ± 4.3	20.2 ± 14.7	68.2 ± 13.6
^{93}Sr	445.4	26.1 ± 17.9	40.9 ± 9.4	42.2 ± 7.7	26.3 ± 17.7	64.1 ± 11.5
^{94}Sr	75.3	43.4 ± 38.6	48.5 ± 9.7	52.2 ± 10.6	43.4 ± 38.6	55.2 ± 9.9
^{95}Sr	23.9	66.7 ± 34.6	35.0 ± 8.8	30.6 ± 6.1	67.5 ± 35.1	37.3 ± 8.9
^{96}Sr	1.1	33.6 ± 8.33	21.8 ± 7.8	15.8 ± 3.8	35.3 ± 8.8	22.1 ± 8.0
^{97}Sr	0.4	5.51 ± 1.55	6.69 ± 4.01	4.76 ± 1.17	5.51 ± 1.55	6.73 ± 3.97
^{98}Sr	0.7	1.22 ± 0.33	1.75 ± 1.85	1.30 ± 0.37	1.22 ± 0.32	1.75 ± 1.85
^{99}Sr	0.3	0.42 ± 0.11	0.26 ± 0.50	0.20 ± 0.06	0.42 ± 0.11	0.05 ± 0.05

Table 13. Yields of palladium isotopes and comparison with systematics. In this case, the cumulative yields of the palladium are obtained in the analysis ($Y_{\text{cumul}} = Y_{\text{indep}}$), see section 5.10 for details.

Isotope	Independent yield				Cumulative yield	
	Half-life	This work	Z_p-model	Grashin's model	This work	Z_p-model
	(s)	0.01%	0.01%	0.01%	0.01%	0.01%
^{113}Pd	93.0	2.24 ± 1.44	1.47 ± 0.88	2.44 ± 1.97	2.24 ± 1.44	4.39 ± 2.37
^{114}Pd	145.2	2.34 ± 1.52	1.52 ± 1.42	3.91 ± 3.11	2.34 ± 1.52	4.30 ± 2.32
^{115m}Pd	50.0	2.31 ± 1.53			2.31 ± 1.53	
^{115}Pd	25.0	0.96 ± 0.57	2.82 ± 1.55	3.42 ± 2.75	0.96 ± 0.57	3.57 ± 1.89
^{116}Pd	12.4	2.11 ± 1.46	2.11 ± 1.20	2.83 ± 2.23	2.11 ± 1.46	2.33 ± 1.23
^{117}Pd	4.3	0.46 ± 0.33	1.07 ± 0.68	1.76 ± 1.36	0.46 ± 0.33	1.11 ± 0.68

Table 14. Yields of silver isotopes and comparison with systematics.

Isotope	Independent yield				Cumulative yield	
	Half-life	This work	Z_p-model	Grashin's model	This work	Z_p-model
	(s)	0.001%	0.001%	0.001%	0.001%	0.001%
^{113m}Ag	68.7		0.81 ± 1.97		33.9 ± 15.3	8.93 ± 4.91
^{114}Ag	4.6		4.47 ± 3.49	3.26 ± 2.86	28.6 ± 11.8	47.5 ± 25.6
^{115}Ag	1200.0	2.66 ± 2.19	1.99 ± 2.45	9.98 ± 8.54	11.4 ± 8.1	1.99 ± 2.45
^{115m}Ag	18.0		10.7 ± 13.2		25.2 ± 18.6	46.4 ± 24.6
^{116m}Ag	160.8	8.01 ± 5.02	9.04 ± 10.1		8.01 ± 5.02	9.04 ± 10.1
^{116}Ag	8.2		14.1 ± 15.8	16.4 ± 14.2	13.2 ± 2.6	37.6 ± 20.3
^{117m}Ag	5.3	20.7 ± 9.6	23.8 ± 26.1		27.6 ± 12.6	29.3 ± 26.4
^{117}Ag	73.6	15.7 ± 13.4	4.43 ± 4.87	21.4 ± 18.2	18.8 ± 15.2	9.99 ± 5.99
^{118m}Ag	2.0	5.43 ± 3.72	11.1 ± 10.6		5.43 ± 3.72	11.1 ± 10.6
^{118}Ag	3.8	67.8 ± 41.8	14.4 ± 16.3	20.3 ± 16.9	67.8 ± 41.8	20.9 ± 16.9
^{119}Ag	2.1	14.7 ± 9.0	13.8 ± 8.43	16.8 ± 13.5	14.7 ± 9.0	14.7 ± 8.5
^{120m}Ag	0.3	19.3 ± 14.0	2.22 ± 3.18	6.77 ± 5.21	19.3 ± 14.0	2.22 ± 3.18
^{120}Ag	1.2		3.47 ± 4.96	4.05 ± 3.12	5.86 ± 3.99	4.44 ± 5.10
^{121}Ag	0.8	5.25 ± 3.26	1.70 ± 1.67	5.85 ± 4.29	5.25 ± 3.26	1.72 ± 1.67
^{122}Ag	5.6	1.18 ± 0.75	0.40 ± 0.64	2.41 ± 1.71	1.18 ± 0.75	0.40 ± 0.64
^{123}Ag	0.3	0.63 ± 0.42	0.83 ± 0.23	0.08 ± 0.23	0.63 ± 0.42	0.08 ± 0.23

Table 15. Yields of cadmium isotopes and comparison with systematics. A different scale is used for Z_p values in the table.

Isotope	Independent yield				Cumulative yield	
	Half-life	This work	Z_p-model	Grashin's model	This work	Z_p-model
	(s)	0.001%	0.00001%	0.001%	0.001%	0.00001%
^{117m}Cd	12096.0	0.62 ± 0.57	630 ± 838	1.32 ± 1.36	1.94 ± 1.73	3930 ± 2320
^{117}Cd	8964.0	2.12 ± 1.93	233 ± 310	0.35 ± 0.36	4.86 ± 4.33	864 ± 648
^{119m}Cd	132.0	0.68 ± 0.71	1710 ± 1950	11.1 ± 10.4	2.12 ± 1.90	020 ± 1960
^{119}Cd	161.4	1.88 ± 1.56	634 ± 723	2.94 ± 2.75	3.28 ± 3.09	1800 ± 988
^{121m}Cd	8.0	2.09 ± 1.59	1210 ± 1450		2.30 ± 1.76	1210 ± 1450
^{121}Cd	13.5	0.95 ± 0.99	447 ± 536	30.2 ± 24.4	1.42 ± 1.57	619 ± 563
^{123m}Cd	1.8	3.62 ± 2.51	317 ± 495		3.62 ± 2.51	317 ± 495
^{123}Cd	2.1	2.10 ± 1.61	200 ± 312	19.9 ± 14.1	2.28 ± 1.70	367 ± 400
^{124}Cd	0.9	11.3 ± 7.8	6.56 ± 44.0	11.3 ± 7.5	11.3 ± 7.77	6.57 ± 44.0
^{125m}Cd	0.6	3.86 ± 2.87	1.31 ± 28.2		3.86 ± 2.87	1.31 ± 28.2
^{125}Cd	0.7	1.54 ± 1.06	0.83 ± 17.8	4.49 ± 2.87	1.54 ± 1.06	1.48 ± 22.7
^{126}Cd	0.5	2.71 ± 1.86	0.53 ± 9.29	1.62 ± 9.72	2.71 ± 1.86	0.53 ± 9.29
^{127}Cd	0.4	2.47 ± 2.06	0.09 ± 2.69	0.41 ± 0.23	2.47 ± 2.06	0.09 ± 2.69

Table 16. Yields of indium isotopes and comparison with systematics.

Isotope	Independent yield				Cumulative yield	
	Half-life	This work	Z_p-model	Grashin's model	This work	Z_p-model
	(s)	0.01%	0.01%	0.01%	0.01%	0.01%
^{119}In	144.0	0.33 ± 0.24	0.38 ± 0.57	0.03 ± 0.04	0.33 ± 0.24	2.54 ± 1.40
^{120m2}In	46.2	0.13 ± 0.09	0.11 ± 0.20		0.13 ± 0.09	0.11 ± 0.20
^{120m}In	47.3	0.21 ± 0.14	0.50 ± 0.95		0.21 ± 0.14	0.50 ± 0.95
^{120}In	3.1	1.04 ± 0.59	0.46 ± 0.88	0.17 ± 0.19	1.04 ± 0.60	0.50 ± 0.95
^{121m}In	226	4.20 ± 7.48	0.34 ± 0.40	0.11 ± 0.11	4.20 ± 7.48	0.74 ± 0.54
^{121}In	23.1	1.45 ± 0.95	1.47 ± 1.75	0.55 ± 0.56	1.45 ± 0.10	2.90 ± 1.65
^{122m2}In	10.3	0.46 ± 0.28	0.25 ± 0.43		0.46 ± 0.28	0.25 ± 0.42
^{122m}In	10.8	0.93 ± 0.60	1.18 ± 2.00		0.93 ± 0.59	1.18 ± 2.00
^{122}In	1.5	4.01 ± 2.67	1.09 ± 1.85	1.69 ± 1.53	4.01 ± 2.67	2.11 ± 2.77
^{123m}In	47.0	0.68 ± 0.47	0.60 ± 0.63	0.51 ± 0.42	0.68 ± 0.47	1.04 ± 0.75
^{123}In	6.0	4.22 ± 2.50	2.63 ± 2.76	2.54 ± 2.07	4.22 ± 2.50	2.71 ± 1.94
^{124m}In	3.7	2.74 ± 1.58	3.35 ± 4.02		2.74 ± 1.58	3.35 ± 4.02
^{124}In	3.2	4.34 ± 2.71	0.80 ± 0.96	3.63 ± 2.72	4.34 ± 2.71	0.81 ± 0.96
^{125m2}In	0.005	1.26 ± 0.80	0.85 ± 1.25		1.26 ± 0.80	0.85 ± 1.25
^{125m}In	0.6	5.21 ± 3.00			5.21 ± 3.00	
^{125}In	12.2	2.19 ± 1.38	3.73 ± 5.48	3.59 ± 2.43	2.19 ± 1.38	3.73 ± 5.48
^{126m}In	1.64	2.78 ± 1.51	3.30 ± 6.93		2.78 ± 1.51	3.30 ± 5.48
^{126}In	1.6	8.90 ± 4.82	0.79 ± 1.66	2.74 ± 1.67	8.90 ± 4.82	0.79 ± 1.66
^{127m}In	3.7	1.94 ± 1.23	0.51 ± 1.66		1.94 ± 1.23	0.51 ± 1.66
^{127}In	1.1	9.04 ± 5.12	2.24 ± 7.30	2.04 ± 1.05	9.04 ± 5.12	2.24 ± 7.30
^{128m}In	0.7	6.06 ± 3.38	0.25 ± 1.33		6.06 ± 3.38	0.25 ± 1.33
^{128}In	0.8	1.40 ± 0.40	1.06 ± 5.67	1.40 ± 0.59	1.40 ± 0.40	1.06 ± 5.67
^{129m}In		1.40 ± 0.81	0.08 ± 0.71		1.40 ± 0.81	0.08 ± 0.71

Table 16. (Continued)

^{129}In	1.78 ± 0.96	0.34 ± 3.10	0.93 ± 0.32	1.78 ± 0.96	0.34 ± 3.10
^{130m}In	0.07 ± 0.04	1.26 ± 5.30		0.07 ± 0.04	1.26 ± 5.30
^{130m2}In	0.18 ± 0.10	0.09 ± 0.40		0.18 ± 0.10	0.09 ± 0.40
^{130}In	0.26 ± 0.14	1.17 ± 4.90	0.48 ± 0.16	0.26 ± 0.14	1.17 ± 4.90
^{131}In	0.15 ± 0.08	0.35 ± 2.94	0.17 ± 0.06	0.15 ± 0.08	0.35 ± 2.94

Table 17. Yields of tin isotopes and comparison with systematics.

Isotope	Independent yield				Cumulative yield	
	Half-life	This work	Z_p-model	Grashin's model	This work	Z_p-model
	(s)	0.1%	0.1%	0.1%	0.1%	0.1%
^{125m}Sn	571.2	0.47 ± 0.30	0.62 ± 0.50	0.07 ± 0.08	2.39 ± 1.09	0.75 ± 0.52
^{127m}Sn	248.0	2.41 ± 0.63	$2.30 \pm \infty$	0.58 ± 0.42	2.70 ± 0.71	2.54 ± 1.55
^{127}Sn	7560.0	4.79 ± 2.03	$3.98 \pm \infty$	1.63 ± 1.16	5.67 ± 2.11	4.02 ± 1.25
^{128m}Sn	6.5	1.50 ± 0.53	$2.52 \pm \infty$		2.10 ± 0.56	2.54 ± 1.57
^{128}Sn	3366.0	11.2 ± 2.9	$6.49 \pm \infty$	4.21 ± 2.20	11.4 ± 2.92	9.14 ± 2.83
^{129m}Sn	435.0	3.36 ± 0.89	$6.18 \pm \infty$	4.12 ± 1.61	3.38 ± 0.89	6.22 ± 4.54
^{129}Sn	133.8	7.78 ± 2.13	$3.90 \pm \infty$	1.47 ± 0.58	8.09 ± 2.21	3.91 ± 2.90
^{130m}Sn	107.0	0.51 ± 0.14	2.89 ± 2.03	4.44 ± 1.31	0.51 ± 0.14	3.02 ± 2.14
^{130}Sn	223.2	10.0 ± 2.5	7.46 ± 5.37	1.63 ± 0.48	10.1 ± 2.5	7.58 ± 5.38
^{131m}Sn	56.0	5.66 ± 1.63			5.66 ± 1.63	
^{131}Sn	58.4	5.15 ± 1.46	1.67 ± 1.95	3.61 ± 1.01	5.25 ± 1.48	1.68 ± 1.96
^{132}Sn	39.7	1.20 ± 0.30	1.20 ± 1.35	1.80 ± 0.73	1.20 ± 0.30	1.98 ± 2.24
^{133}Sn	1.5	0.20 ± 0.08	0.15 ± 0.35	0.27 ± 0.11	0.20 ± 0.08	0.15 ± 0.35

Table 18. Yields of antimony isotopes and comparison with systematics.

Isotope	Independent yield				Cumulative yield	
	Half-life	This work	Z_p-model	Grashin's model	This work	Z_p-model
	(s)	0.1%	0.1%	0.1%	0.1%	0.1%
^{126m}Sb	1170.0	0.06 ± 0.02	0.09 ± 0.41	0.03 ± 0.05	0.06 ± 0.02	4.17 ± 1.29
^{128m}Sb	624.0	2.03 ± 0.52	$0.65 \pm \infty$	1.33 ± 1.23	2.18 ± 0.57	9.78 ± 3.03
^{130m}Sb	2370.0	11.4 ± 5.0	$2.27\pm$		11.4 ± 5.0	9.85 ± 5.52
^{130}Sb	378.0	12.6 ± 3.4	9.70 ± 1.09	16.5 ± 6.1	12.7 ± 3.4	12.7 ± 5.09
^{131}Sb	1381.8	46.2 ± 12.3	17.6 ± 4.65	22.0 ± 5.87	46.3 ± 12.3	22.0 ± 5.28
^{132m}Sb	252.0	5.00 ± 1.40	2.06 ± 4.23		5.01 ± 1.40	2.06 ± 1.26
^{132}Sb	168.0	16.9 ± 4.7	8.81 ± 1.26	15.3 ± 3.7	16.9 ± 4.7	10.0 ± 5.5
^{133}Sb	150.0	11.7 ± 3.2	5.84 ± 5.37	9.41 ± 3.25	11.7 ± 3.2	5.99 ± 2.94
^{134m}Sb	10.4	2.34 ± 1.17	0.04 ± 0.07		2.34 ± 1.17	0.04 ± 0.07
134Sb	0.7	0.71 ± 0.41	0.94 ± 1.82	2.03 ± 0.66	0.71 ± 0.41	0.95 ± 1.82
^{135}Sb	1.8	0.17 ± 0.12	0.22 ± 0.46	0.45 ± 0.18	0.17 ± 0.12	0.22 ± 0.46

Table 19. Yields of tellurium isotopes and comparison with systematics.

Isotope	Independent yield				Cumulative yield	
	Half-life	This work	Z_p-model	Grashin's model	This work	Z_p-model
	(s)	0.1%	0.1%	0.1%	0.1%	0.1%
^{131}Te	1500.0	6.16 ± 5.15	$5.03 \pm \infty$	2.72 ± 1.36	30.1 ± 26.3	28.0 ± 5.9
^{131m2}Te	0.1	4.42 ± 3.67			4.42 ± 3.67	
^{133m}Te	3324.0	87.4 ± 73.2	20.6 ± 8.9	28.6 ± 11.5	87.6 ± 73.4	22.4 ± 8.9
^{133}Te	750.0	14.8 ± 12.3	13.0 ± 5.6	10.2 ± 4.1	15.5 ± 12.8	21.2 ± 6.1
^{134}Te	2508.0	41.4 ± 34.5	30.7 ± 8.3	58.1 ± 19.9	46.8 ± 38.9	32.1 ± 8.7
^{135}Te	19.0	8.57 ± 6.94	13.2 ± 5.7	18.3 ± 5.5	9.23 ± 7.45	13.4 ± 5.8
^{136}Te	13.6	3.12 ± 2.58	4.05 ± 3.32	6.41 ± 2.41	31.2 ± 2.58	4.06 ± 3.3
^{137}Te	2.5	2.16 ± 1.75	0.56 ± 0.97	1.07 ± 0.38	2.16 ± 1.75	0.58 ± 0.97

Table 20. Yields of iodine isotopes and comparison with systematics.

Isotope	Independent yield				Cumulative yield	
	Half-life	This work	Z_p-model	Grashin's model	This work	Z_p-model
	(s)	0.1%	0.1%	0.1%	0.1%	0.1%
^{133m}I	9.0	0.93 ± 0.24	1.65 ± 1.26	4.13 ± 1.63	1.23 ± 0.35	1.65 ± 1.26
^{134m}I	221.0	7.99 ± 1.85	35.7 ± 9.3	10.4 ± 3.4	7.99 ± 1.85	35.7 ± 9.3
^{134}I	3156.0	89.0 ± 32.5	15.6 ± 7.79	11.7 ± 3.8	91.6 ± 33.1	50.6 ± 9.6
^{135}I	23652.0	49.4 ± 10.7	31.9 ± 6.38	51.8 ± 13.3	49.6 ± 10.7	45.4 ± 8.6
^{136m}I	46.9	5.24 ± 1.15	8.70 ± 4.26		5.24 ± 1.15	8.70 ± 4.26
^{136}I	83.4	8.35 ± 13.4	13.6 ± 6.7	33.4 ± 7.9	8.53 ± 13.4	17.6 ± 7.4
^{137}I	24.1	9.74 ± 2.21	13.6 ± 5.0	16.4 ± 4.8	9.85 ± 2.23	14.1 ± 5.1
^{138}I	6.5	4.19 ± 1.26	3.78 ± 2.50	4.40 ± 1.22	4.19 ± 1.26	3.84 ± 2.50
^{139}I	2.3	1.06 ± 0.52	0.99 ± 1.30	1.11 ± 0.34	1.06 ± 0.52	0.99 ± 1.30
^{140}I	0.9	0.90 ± 0.44	0.10 ± 0.28	0.19 ± 0.06	0.90 ± 0.44	0.10 ± 0.28

Table 21. Yields of xenon isotopes and comparison with systematics.

Isotope	Independent yield				Cumulative yield	
	Half-life	This work	Z_p-model	Grashin's model	This work	Z_p-model
	(s)	0.1%	0.1%	0.1%	0.1%	0.1%
^{135m}Xe	918.0	2.15 ± 5.68	7.78 ± 6.93	5.54 ± 1.94	22.6 ± 5.9	14.2 ± 6.8
^{135}Xe	32904.0	5.30 ± 14.1	4.91 ± 4.37	1.98 ± 0.69	54.7 ± 14.5	58.0 ± 10.4
^{137}Xe	229.1	77.2 ± 55.2	43.2 ± 9.1	48.4 ± 12.1	77.2 ± 55.2	56.5 ± 10.2
^{138}Xe	844.8	70.1 ± 18.1	47.0 ± 10.3	55.8 ± 15.0	70.2 ± 18.2	50.7 ± 10.6
^{139}Xe	39.7	35.2 ± 12.4	28.9 ± 8.9	24.0 ± 5.8	35.3 ± 12.4	29.8 ± 8.9
^{140}Xe	13.6	12.1 ± 5.6	13.6 ± 7.1	10.2 ± 2.3	12.1 ± 5.6	13.7 ± 7.0
^{141}Xe	1.7	3.42 ± 2.09	2.63 ± 2.63	2.85 ± 0.86	3.42 ± 2.09	2.64 ± 2.64

Table 22. Yields of cesium isotopes and comparison with systematics.

Isotope	Independent yield				Cumulative yield	
	Half-life	This work	Z_p-model	Grashin's model	This work	Z_p-model
	(s)	0.1%	0.1%	0.1%	0.1%	0.1%
^{134m}Cs	10476.0	0.007 ± 0.003		0.008 ± 0.004	0.007 ± 0.003	
^{135m}Cs	3180.0	0.03 ± 0.01	0.03 ± 0.15	0.03 ± 0.01	0.03 ± 0.01	0.03 ± 0.15
^{136m}Cs	19.0	0.75 ± 0.36			0.75 ± 0.36	
^{138m}Cs	174.0	10.7 ± 5.4	5.61 ± 3.64	10.6 ± 2.2	10.7 ± 5.4	5.61 ± 3.64
^{138}Cs	2004.6	23.1 ± 11.2	8.75 ± 5.7	6.32 ± 1.29	23.7 ± 11.5	64.0 ± 10.9
^{139}Cs	556.2	39.2 ± 18.7	32.8 ± 7.5	35.1 ± 6.0	40.1 ± 19.1	62.6 ± 11.9
^{140}Cs	63.7	33.6 ± 30.1	33.6 ± 6.7	28.2 ± 4.7	37.5 ± 32.4	47.3 ± 9.9
^{141}Cs	24.9	28.3 ± 13.5	26.7 ± 7.0	18.3 ± 3.9	28.4 ± 13.5	29.4 ± 7.3
^{142}Cs	1.7	6.44 ± 3.38	9.21 ± 3.78	7.88 ± 1.89	6.44 ± 3.38	9.56 ± 3.83
^{143}Cs	1.8	5.66 ± 2.65	3.00 ± 2.28	2.70 ± 7.29	5.66 ± 2.65	3.02 ± 2.29
^{144}Cs	1.0	1.27 ± 0.59	0.39 ± 0.62	0.60 ± 0.17	1.27 ± 0.59	0.39 ± 0.62
^{145}Cs	0.6	0.17 ± 0.08	0.04 ± 0.12	0.12 ± 0.04	0.17 ± 0.08	0.04 ± 0.20
^{146}Cs	0.3	0.02 ± 0.01	0.001 ± 0.008	0.02 ± 0.01	0.02 ± 0.01	0.001 ± 0.008

Table 23. Yields of barium isotopes and comparison with systematics.

Isotope	Independent yield				Cumulative yield	
	Half-life	This work	Z_p-model	Grashin's model	This work	Z_p-model
	(s)	0.1%	0.1%	0.1%	0.1%	0.1%
^{137m}Ba	153.1	0.14 ± 0.04	0.08 ± 0.47		0.14 ± 0.04	0.08 ± 0.47
^{139}Ba	4983.6	19.1 ± 5.9	5.33 ± 3.95	4.64 ± 1.15	78.6 ± 32.9	67.9 ± 10.9
^{141}Ba	1096.2	62.4 ± 18.9	35.4 ± 9.2	29.4 ± 4.0	101.0 ± 28.3	64.7 ± 12.3
^{142}Ba	636.0	87.2 ± 24.3	47.0 ± 9.9	40.3 ± 7.6	95.8 ± 26.6	56.6 ± 10.8
^{143}Ba	14.3	14.1 ± 5.4	35.6 ± 8.2	27.4 ± 6.0	18.4 ± 6.1	38.6 ± 8.5
^{144}Ba	11.5	8.79 ± 3.63	21.2 ± 7.2	14.6 ± 3.7	10.4 ± 4.0	21.5 ± 7.1
^{145}Ba	4.3	2.39 ± 1.54	5.32 ± 3.14	4.80 ± 1.23	2.58 ± 1.53	5.35 ± 3.16
^{146}Ba	2.2	1.62 ± 1.07	0.89 ± 1.05	1.46 ± 0.41	1.62 ± 1.07	0.89 ± 1.05
^{147}Ba	0.9	0.19 ± 0.15	0.06 ± 0.16	0.27 ± 0.08	0.19 ± 0.15	0.06 ± 0.16

Table 24. Comparison of the charge yield $Y(Z)$ of complementary charges.

Pair of complementary charges	$Y(Z_{\text{light}})$ per fission	$Y(Z_{\text{heavy}})$ per fission
^{38}(Sr)/^{54}(Xe)	$(1.97 \pm 1.15) \cdot 10^{-1}$	$(2.06 \pm 1.40) \cdot 10^{-1}$
^{37}(Rb)/^{55}(Cs)	$1.43.10^{-1} \pm 6.74 \cdot 10^{-2}$	$1.49 \cdot 10^{-1} \pm 8.6 \cdot 10^{-2}$
^{36}(Kr)/^{56}(Ba)	$2.01 \cdot 10^{-1} \pm 5.19 \cdot 10^{-2}$	$1.96 \cdot 10^{-1} \pm 6.10 \cdot 10^{-2}$

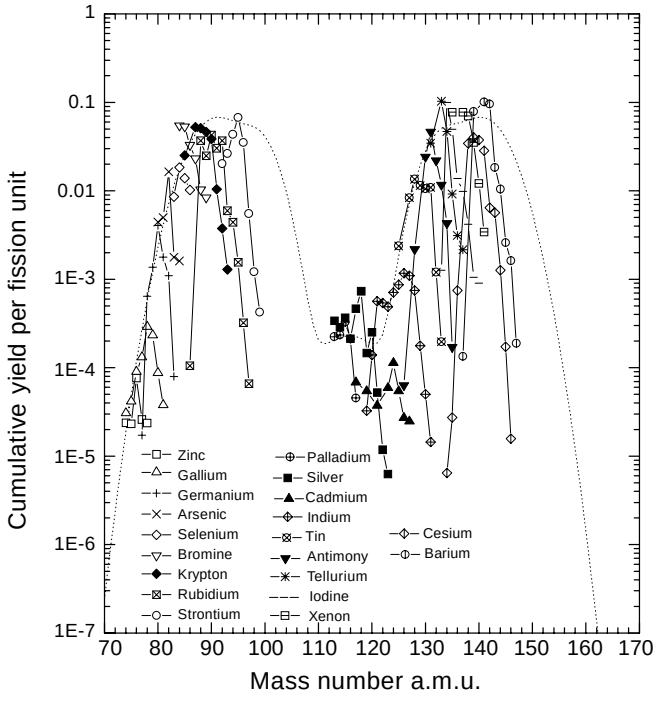

Fig. 4. Cumulative yield curves. Yields of isotopes belonging to the same element are joined by a straight line. The mass distribution obtained by Wahl's model [17] is shown by a dotted line.

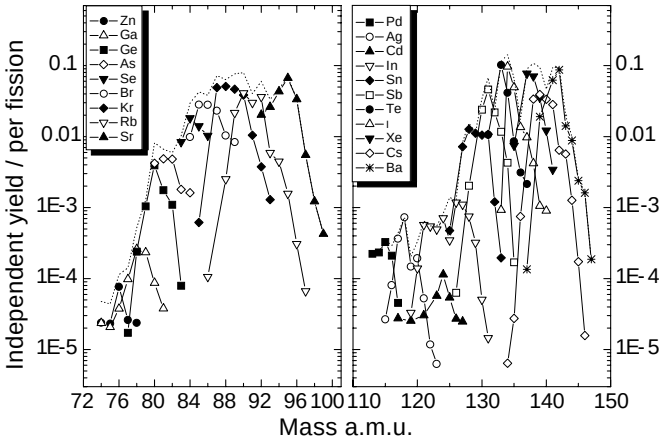

Fig. 5. Independent isotopic yields in the fast neutron induced fission of ^{233}U. The dotted line represents the total mass yield.

The mass yield distribution obtained by the empirical mass distribution model of Wahl [18] has also been plotted in fig. 4. The corresponding curves should envelop the cumulative yield curves. This is found to be the case with a small number of exceptions.

The isotopic distributions in fig. 4. are quite regular, and the plots can be used to estimate the yields of nuclides not included in the measurements.

6.2 Independent yields

The on-line technique for the fission yield measurements has the advantage of being sensitive (yield values down to 10^{-4}% can be determined in fast fission) and fast enough to make it possible to observe very short-lived products on the extreme neutron-rich side of the mass distribution can be observed. About 200 independent yields are reported in this work. A significant amount of isomeric yields has been determined as well. This will be discussed in a following subsection.

In the light peak region, data from mass 74 to mass 99 were obtained, covering a nuclear charge from 30 (Zn) to 38 (Sr). The independent yields measured in this region are given in fig. 5 (isomeric state yields are added when encountered).

In the heavy region, we have been able to obtain data at OSIRIS on masses from 113 to 147, within a nuclear charge range from 46 (Pd) to 56 (Ba). The elements from Y ($Z = 39$) to Rh ($Z = 45$) can however not be obtained on-line. Moreover, the separation efficiency for lanthanides was much too low to allow efficient measurements for the fast fission of ^{233}U. In principle, the lanthanides can be separated efficiently by the use of CF_4 as a carrier gas in a different type of ion source. The practical application of such a method was precluded by the scarcity of the ^{233}U target material. Moreover, the nuclear data of the region is too poorly known for analysis by means of gamma-ray assay.

A small odd-even effect can be recognized by inspecting the yield distribution for different isotopes. This is seen mostly from the fact that yield of even nuclear charge, given by black symbols in fig. 5, approaches systematically more closely to the total mass yield than the odd charges. The result is in agreement with systematics, where, for far asymmetric fission, the odd-even effects for the protons increases. This will be further discussed in section 6.3.

In the following, we compare the mass yield before delayed neutron emission $Y(A) = \sum_{Z,I} Y(A, Z, I)$ and the charge yield $Y(A) = \sum_{A,I} Y(A, Z, I)$ obtained in this work with the mass and charge distributions estimated by Wahl, in order to illustrate their systematic trends. Figure 6 shows that the estimates of Wahl agree quite well with the measured values. Both the measured values and the estimates can be observed to follow similar trends in the region of symmetry of the charge distribution from the charge $Z = 46$ (Pd) to $Z = 49$ (In). The measured values appear to have a slightly higher yield than the estimates from the Z_p-model. This can be explained by the fact that the model values are rather uncertain in the symmetry region due to the lack of experimental data here.

One has to note that in the present experiment many mass yields have been measured in the valley region, *viz.* from mass $A = 113$ to about $A = 123$. Such data are scarce since most methods of fission yield measurements do not access this region for the independent yields. Hence, this kind of information is practically only accessible by ISOL technique combined with γ-spectroscopy, as in the present work. In the $Y(A)$ representation of fig. 6, the true mass yield (*i.e.* the sum of independent yields) is plotted for the OSIRIS values. In the upper edges of the mass

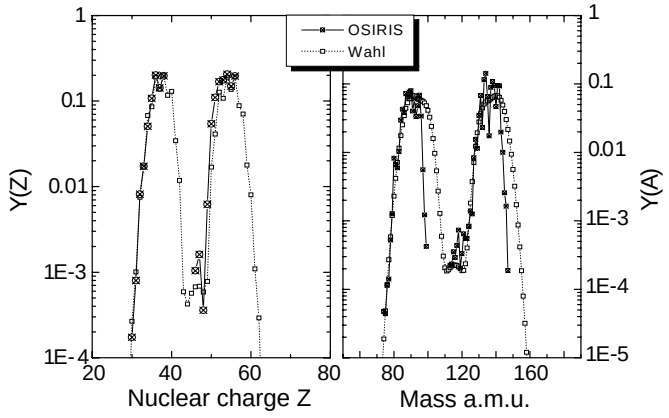

Fig. 6. Mass (right side) and charge distribution (left side) of the fission yields measured with OSIRIS in the ^{233}U(n$_{\rm f}$, f) reaction. These summations are compared with the Wahl's estimated overall mass and charge distributions of the fission products.

distribution (*i.e.* from about mass $A = 97$ to $A = 99$ for the light peak and from about $A = 144$ to $A = 147$ for the heavy peak), not all elements of an isobaric chain can be measured due to the limitations of the method (some elements are not evaporated from the target). Thus, the measured mass yield for these isobars cannot be compared to the mass chain yield estimated by the model, since they are not supposed to be equal anymore.

In the experimental mass distribution, peaks can be observed at the following mass numbers: $A_{\rm light} = 90$, 92 and $A_{\rm heavy} = 139$, 141. If the most probable masses are added, one obtains

$$A_{\rm light} + A_{\rm heavy} = 231 \tag{2}$$

which means that three neutrons on average have been evaporated, *i.e.* $A_{\rm light} + A_{\rm heavy} + 3n = {}^{234}$U for the considered masses. This observation agrees with the estimate [18] of the average number of emitted neutrons per fission, $\nu_{\rm p} = 2.61$, for the fast fission reaction of ^{233}U. As a validation of the measured data, one may compare the charge balance through the yields of two complementary fragment charges ($Z_{\rm light} + Z_{\rm heavy} = 92$). Actually, only three pairs $Z_{\rm light}/Z_{\rm heavy}$ of complementary charges are accessible by the OSIRIS technique, *viz.* 54/38, 55/37 and 56/36. Table 24 shows the quite good agreement found between those yield values.

6.3 Odd-even effect

Odd-even effects in the yield distribution are normally understood as a preferential formation of fission products with even atomic number (Z) (or even neutron number, N) relative to odd fission products [27,28] They have been interpreted as a consequence of the preservation of nuclear pairing (superfluidity) in the fissioning nuclei on the way from the saddle point to scission and, hence, of an adiabatic character of the fission leading to a low internal excitation energy at scission [16,17] (Note that some caution is needed: Odd-even effects have been observed in nearly all low-energy fission processes of even-Z nuclei with $A =$ 230–250 [16,17,29]. However, the reasoning given here is not applicable to a system that already has an unpaired nucleon in the ground state. In such cases a different interpretation [30] is needed.)

In reality, the emission of prompt neutrons from the fission fragments does not allow studies where primary fragments are involved. It is therefore useful to use the charge distribution $Y(A) = \sum_{A,I} Y(A, Z, I)$, a quantity which is not affected by the neutron evaporation cascade.

In the charge distribution of fig. 6, a simple and appealing structure shows up with even-Z yields ($Z_{\rm light} = 36$, 38 and $Z_{\rm heavy} = 54$, 56; $Z_{\rm light} + Z_{\rm heavy} = 92$ (U)) being systematically enhanced compared to odd-Z yields. This odd-even staggering is known to be characteristic of the proton, or charge, odd-even effect in the yields of fission products. Of course, more detailed insight into the odd-even effect is gained by studying the independent yields for each isotope $Y(A, Z) = \sum_I Y(A, Z, I)$ for each element Z, as plotted in fig. 5 where the proton odd-even effect becomes visible upon the independent yields. Indeed, depending on the odd-even character of the isobar A, the usually dominating proton odd-even effect is modulated by the neutron odd-even effect in the isobaric distribution $Y(Z|A)$, while in the isotopic distribution $Y(A|Z)$ only the neutron odd-even effect will come into play.

It is customary to evaluate the amplitude of the odd-even effect in the charge yield for even and odd charge splits Ye and $Y_{\rm o}$, respectively:

$$\delta_{\rm p} = \frac{Y_{\rm e} - Y_{\rm o}}{Y_{\rm e} + Y_{\rm o}}. \tag{3}$$

The proton odd-even effect for the ^{233}U(n$_{\rm f}$, f) reaction is found to be $\delta_{\rm p} = 0.178 \pm 0.072$ (as a comparison for the thermal fission of ^{233}U, $\delta_{\rm p}$ was found to be equal to 0.221 ± 0.021 [31] by Quade and 0.198 ± 0.028 by Rudstam [24].

One can use the odd-even effect $\delta_{\rm p}$ to probe the intrinsic excitation energy of the fissioning system, as it has been reviewed in ref. [32] A model has been proposed by Nifenecker *et al.* [33], in which the odd-even effect is calculated from a combinatorial analysis of pair breaking, with the maximum of number of broken pairs depending on the available heat energy. Under some simplifying assumptions it may be shown [34,35], that within the framework of Nifenecker model the following relation between the prescission excitation energy $E_{\rm XPS}$ and the odd-even effect $\delta_{\rm p}$ holds:

$$E_{\rm XPS}\,({\rm MeV}) \approx -4 \ln \delta_{\rm p}. \tag{4}$$

Bearing in mind that both the excitation energy $E_{\rm XSAD}$ already present at the saddle point and the energy $E_{\rm DIS}$ dissipated through viscous forces in course of fission between saddle and scission point will contribute to $E_{\rm XPS}$, one has

$$E_{\rm XPS} = E_{\rm XSAD} + E_{\rm DIS}. \tag{5}$$

For neutron-induced fission, the excitation energy $E_{\rm XSAD}$ may be approximated by

$$E_{\rm XSAD} = B_{\rm n} - B_{\rm f} + E_{\rm n}. \tag{6}$$

Table 25. Prescission excitation energy E_{XPS}, excitation energy E_{XSAD} and dissipation energy E_{DIS} deduced from the odd-effect for the ^{233}U(n, f) reaction. The second fission barrier height $E_{\mathrm{f}} = 5.5$ MeV and the neutron binding energy $B_{\mathrm{n}} = 6.84$ MeV have been used.

	^{233}U(n_f, f) Present work	^{233}U(n_{th}, f) from Rudstam *et al.* [11]	^{233}U(n_{th}, f) from Quade *et al.* [31]
E_{XPS} (MeV)	6.90	6.48	6.03
E_{XSAD} (MeV)	2.54	1.34	1.34
E_{DIS} (MeV)	4.36	5.14	4.69

Table 26. Comparison between ^{233}U, ^{235}U and ^{238}U fiiy-values.

		Experimental fiiy(%)		
Spin	Nuclide	^{233}U	^{235}U	^{238}U
		Odd-Mass Nuclides		
$\frac{9}{2}$	^{81}Ge	76 ± 7	70 ± 6	54 ± 8
$\frac{1}{2}$		24 ± 7	30 ± 6	46 ± 8
$\frac{9}{2}$	^{127}In	82 ± 4	87 ± 6	67 ± 9
$\frac{1}{2}$		18 ± 4	13 ± 6	33 ± 9
$\frac{9}{2}$	^{129}In	56 ± 9	76 ± 7	60 ± 8
$\frac{1}{2}$		44 ± 9	24 ± 7	40 ± 8
$\frac{11}{2}$	^{123}Cd	63 ± 7	68 ± 2	70 ± 12
$\frac{3}{2}$		37 ± 7	32 ± 2	30 ± 12
$\frac{11}{2}$	^{125}Cd	71 ± 9	66 ± 8	91 ± 6
$\frac{3}{2}$		29 ± 9	34 ± 8	9 ± 6
$\frac{11}{2}$	^{129}Sn	31 ± 10	43 ± 6	57 ± 6
$\frac{3}{2}$		69 ± 10	57 ± 6	43 ± 6
$\frac{11}{2}$	^{133}Te	86 ± 7	78 ± 4	87 ± 5
$\frac{3}{2}$		14 ± 7	22 ± 4	13 ± 5
		Even-Mass Nuclides		
4	^{90}Rb	66 ± 6	58 ± 5	38 ± 5
1		34 ± 6	42 ± 5	62 ± 5
5	^{82}As	13 ± 8	17 ± 7	8 ± 4
2		87 ± 8	83 ± 7	92 ± 4
6	^{120}Ag	96 ± 20	85 ± 15	86 ± 4
3		4 ± 20	15 ± 15	14 ± 4
6	^{138}Cs	31 ± 10	58 ± 8	19 ± 3
3		69 ± 10	42 ± 8	81 ± 3
7	^{130}Sn	5 ± 15	13 ± 2	14 ± 2
0		95 ± 15	87 ± 2	86 ± 2
8	^{126}In	23 ± 7	30 ± 7	36 ± 7
3		77 ± 7	70 ± 7	64 ± 7
8	^{134}I	8 ± 16	20 ± 2	10 ± 3
4		92 ± 16	80 ± 2	90 ± 3
		Nuclides with two isomeric states in addition to the ground state		
$\frac{21}{2}$	^{131}In		0.40 ± 0.17	3.5 ± 1.3
$\frac{9}{2}$		N/A	16 ± 7	21 ± 6
$\frac{1}{2}$			83 ± 7	75 ± 7
12	^{130}In	22 ± 10	24 ± 4	25 ± 5
5		50 ± 10	44 ± 5	41 ± 7
2		28 ± 10	32 ± 4	34 ± 7

In this equation, B_n and E_n are the binding and kinetic energy of the incident neutron, respectively, and B_f is the fission barrier height. Rather arbitrary, from the double-humped barrier structure the higher of the two barriers is usually chosen. As a further approximation, no energy gap in the saddle is taken into account below which quasi particle excitations are ruled out.

Inserting the appropriate numbers in eqs. (3)–(6), the energy E_{DIS} dissipated between the saddle and scission point, may be evaluated for thermal [24,31] and fast fission of ^{233}U (present work). The results, shown in table 25, suggest nearly equal dissipation energies in these reactions.

6.4 Isomeric Yields

The present work has contributed an extensive set of measurement of isomeric yields. The division of the independent isotopic yield on the isomeric states of a nuclide has always been a problem in fission yield estimates. There are attempts to predict this property using extrapolations from known cases, for instance by Madland and England [36] and by Rudstam [37]. None of these attempts is altogether satisfactory, and it is therefore important to enlarge and further scrutinize the experimental database available as a basis to improve the predictions. The partition on isomeric states is assumed to be coupled to the angular momenta of isomers but, so far, there have been rather few cases available for testing the theoretical models. The present study provides 62 measurements of isomeric states over pairs and triplets, which is a considerable extension of the material available until now.

A highly significant intercomparison can be obtained through the isomeric yields from thermal fission of ^{235}U [12], from fast fission of ^{238}U and from fast fission of ^{233}U, all measured at Studsvik. The three measurements do not overlap with regard to all isomeric yield values. Consequently, only a subset of the isomeric yields can be given in table 26. The table shows a remarkably good agreement between the (= fractional independent isomeric yield) values from the three systems. In most of the cases the differences is within or close to the combined limit of the errors.

Rudstam has pointed out [38] the striking case of ^{138}Cs where the isomeric partition values from ^{235}U and ^{238}U were strongly different, see also table 26. This case may not be too significant, however, since the ground-state independent yield is difficult to determine due to a very large cumulative yield. Actually, the independent ground state yield for ^{235}U in that comparison [38] had been obtained by an indirect method. The present data for fast fission of ^{233}U suggest that most of the independent population goes to the ground state of ^{138}Cs, as was also seen in the ^{238}U fission reaction.

It is very interesting to note the generally highly similar fiiy values for the three fissioning systems, since they have rather different angular momenta. This indicates that the partition on the isomeric states is much more related to the nuclear properties of the individual fission products than to the dynamics of the fission process itself, which may be an important consideration in attempts to model the yield distribution.

6.5 Comparison of the thermal and fast neutron induced fission of ^{233}U measured at OSIRIS

The main differences between fast and thermal fission are expected to occur at the outer flanks of the mass distribution and in the valley region. The supplement of neutron energy progressively increases the temperature of the system and makes it less sensitive to the shell structure of the compound nucleus. If the excitation energy for induced fission is increased (*e.g.* for 14 MeV neutron energy), one would observe that the mass distribution becomes wider and shifts smoothly to the light masses. This effect comes from the fact that the fission fragments evaporate a larger number of neutrons. At high energy ($E^* > 50$ MeV), a symmetric distribution of the fission products is expected because the "liquid drop" characteristic of the hot nuclear material dominates completely over the shell structure.

The differences of mass symmetry yields for different incident neutron energy can be significant, *e.g.* in the ^{235}U(n, f) reaction these yields are increased by more than two orders of magnitude for neutron energies raising from thermal to 14 MeV. Compared to this dramatic variation, the changes in other characteristics of the distribution are only minor: with the increasing excitation energy the average mass number in the light group stays about constant while the one in the heavy group is shifted downwards (indicating the increase in neutron emission with increasing energy is larger for heavy fragment).

On should mention as well that a drastic decrease of the odd-even effect for an increase in excitation energy of the compound system has been observed [39,40].

The data for the thermal and fast fission of ^{233}U measured at Studsvik with the OSIRIS facility are compared in fig. 7. The thermal yields come from an experiment carried out by G. Rudstam *et al.* [24] and the fast ones are from the present work. These two experiments do not use precisely identical nuclear data for the yield derivations, but the differences are negligible for the present discussion. The right wing of the valley region (symmetric fission) has been encircled in the figure, where the yields are seen to increase with increasing energy of the incident neutron. This is actually the expected behavior of the mass distribution $Y(A)$. A similar behavior in the charge distribution is observed, even if it is less pronounced.

The observations regarding the odd-even effect δ_p for both experimental sets of data has been discussed in subsection 6.3.

6.6 Analysis in term of fission modes

The multi-modal random neck-rupture of Brosa [41] deduces the fission characteristics from the properties of the scission configuration alone, by predicting the existence of several modes in the potential energy landscape

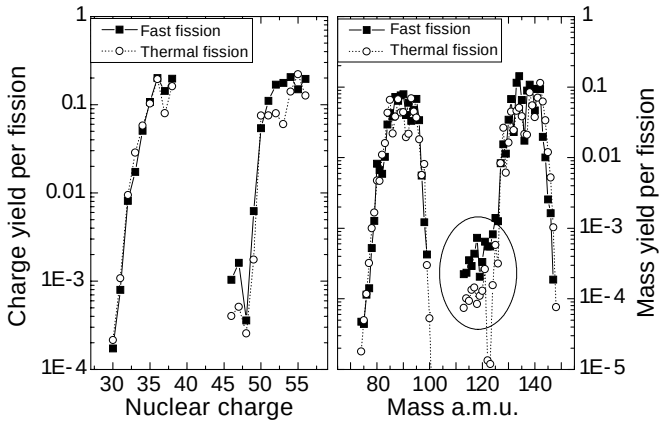

Fig. 7. Comparison of the mass and charge distribution behavior of the thermal and fast neutron-induced fission of ^{233}U.

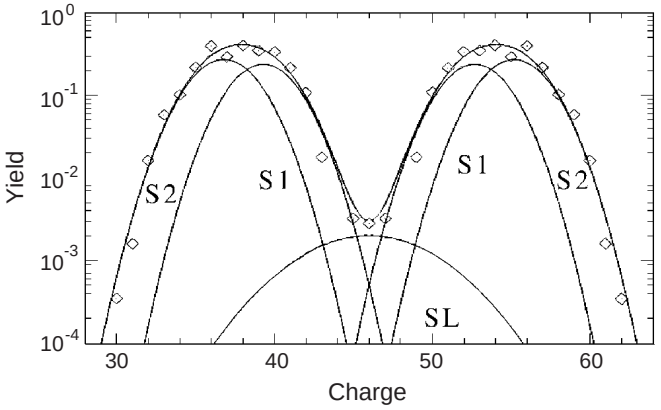

Fig. 8. The symmetrized data from the present work is shown together with fitted Gaussian distributions representing the three fission modes of interest in the Brosa model. See section 7 in the text for details.

leading to different scission shapes of the compound nucleus. However, and importantly, this approach neglects the dynamic evolution of the system from the saddle to scission. The concept of independent fission channels has been proposed as a consequence of having the fissioning system following specific valleys in the potential energy in the direction of elongation. Several properties (*e.g.*, average mass or charge split, mass and charge width, and main total kinetic energy) can be related to calculated properties of the highly deformed fissioning system. This model is commonly applied to describe the two-dimensional $Y(Z, TKE)$ distribution, which provides a vast amount of physical information on the splitting of the compound system.

A first idea of the location of the fission modes can be obtained using the one-dimensional charge distribution extracted from the symmetrized fission yield data of ^{233}U$(\mathrm{n_f}, \mathrm{f})$. The data were symmetrized by extrapolating missing values by the symmetry properties of the two mass yield peaks.

Hence, the parameterization of the distribution shown in fig. 8 by Gaussian functions (as derived from the data) provides $Z_1 = 52.7$, $Z_2 = 55.2$, $Z_\mathrm{L} = 46$, respectively as central values for each Gaussian representing the nuclear-charge yields for each fission mode. According to the terminology introduced by Brosa *et al.* [41], the labeling of the standard modes has been done in a growing order of the asymmetry of the modes. Thus, S1 (standard I) is the least asymmetric and S2 (standard II) is the most asymmetric one. The mode labeled SL, which means superlong, is related to the symmetric scission configuration of the compound nucleus.

One should notice that the mean position of the Gaussian functions found in the ^{233}U$(\mathrm{n_f}, \mathrm{f})$ study is in very good agreement with the fission mode study of a secondary beam of ^{234}U [42] by the method of fission in inverse kinematics. This latter experiment imparted only a modestly higher (~ 4 MeV) excitation in the fissioning system than that of the present work.

A study of the multi-mode theory for neutron induced fission of actinide nuclei by Tie-shuan fan *et al.* [43] led to an empirical prediction of the mode probabilities as a function of increasing excitation energy directly related to the incident kinetic neutron energy E_n, as given by the following equations:

$$W_i = A_i + B_i \times \exp(C_i \times E_\mathrm{n}(\,\mathrm{MeV})), \qquad (7)$$

where W_i is the channel probability, A_i, B_i and C_i are free parameters for the fission mode i. The values obtained by fitting to the available experimental data [43] are given in table 27.

With these parameter values, the intensities obtained for each mode as a function of energy are given in table 28.

The thermal values can be compared to the experimental fitted values from ref. [44] giving the yield associated to the standard 1 and standard 2 modes, respectively $Y(\mathrm{S1}) = 4\%$ and $Y(\mathrm{S2}) = 96\%$. The superlong mode was neglected in fitting because of the very small proportion of symmetric fission in the thermal neutron-induced fission of uranium.

From the present ^{233}U$(\mathrm{n_f}, \mathrm{f})$ distribution, the yields corresponding to each mode are deduced as $Y(\mathrm{S1}) = 44\%$,

Table 27. Fitting parameters of three fission modes for ^{234}U fissioning nucleus [42].

Modes	A_i	B_i	C_i	E_n range (MeV)
Standard 2	101.1	−11.0	0.12	
Standard 1	−43.6	−53.1	0.02	thermal −5.5
Superlong	−0.53	0.80	0.30	

Table 28. Mode intensities obtained for the ^{234}U fissioning nucleus using the empirical relation of eq. (7).

E_n	Standard 2	Standard 1	Superlong
thermal	90%	9.5%	0.5%
1.4 (MeV)	88%	11%	1%
4.1 (MeV)	82%	15.7%	2.3%

Table 29. Comparison of the intensities of the different modes in the fission of the compound nucleus ^{234}U from OSIRIS experiment, secondary beam experiment and empirical calculations.

	Standard 2(%)	Standard 1(%)	Superlong (%)
OSIRIS measurement	55	44	1
Secondary beam measurement	39.1	49.7	11.2
Calculated values $E_n = 1.4$ MeV	88	11	1

$Y(\mathrm{S2}) = 55\%$ and $Y(\mathrm{SL}) = 1\%$. These values are compared in table 29 to the ones calculated using eq. (7) and to the deduced intensities from fission with a secondary beam of ^{234}U.

Even if the superlong mode has a low contribution, it can be observed, showing an increase of the symmetric yields when going from thermal to fast fission. Here again a good agreement is observed between the data measured with OSIRIS ($E^*(^{234}\mathrm{U}) \approx 8.04$ MeV) and the study by Schmidt *et al.* [42] in the secondary beam experiment ($E^*(^{234}\mathrm{U}) \approx 11$ MeV). The discrepancy in the intensities observed for the superlong mode is understandable, since it has been observed in the previous studies of neutron-induced fission of ^{238}U [45], that the superlong mode *increases exponentially* as a function of the increase of the excitation energy of the compound nucleus (effect of the liquid drop). On the other hand, the standard 2 tends to decrease, whereas the standard 1 increases (shell effect), with higher excitation energy of the system.

7 Conclusion

The purpose of this work was to improve the experimental nuclear data on fission product yields for the $^{233}\mathrm{U}(\mathrm{n_f}, \mathrm{f})$ reaction. The experiment has been performed using the mass separator OSIRIS (Isotope Separator On-Line type) located in Studsvik (Sweden). The measurements of the fission products are done by combining the mass separation with γ-ray spectroscopy. OSIRIS is one of the few facilities in the world, if not the only one, where this technique can be applied currently. Despite the limitations of the integrated target ion-source efficiency, one can successfully measure a large part of the independent yield distribution (both light and heavy mass peak regions) including many isomeric pairs and the region of symmetry. The information on both the distribution of independent yields among isomeric states and charge distribution in the region of symmetry is scarce so far, as these values are practically inaccessible to most other techniques. With these features, the OSIRIS method complements the high resolution fission recoil techniques which limited to the measurement of the light mass region independent yields, and the radiochemical techniques used mainly for the determination of the mass chain yields.

The measurement of both independent and cumulative yields of about 180 nuclides covering most of the yield distribution, including many isomeric states, is reported here. The investigated yields include nuclides from Zinc ($Z = 30$) to Strontium ($Z = 38$) in the mass-range 74–99 and nuclides from Palladium ($Z = 46$) to Barium ($Z = 56$) in the mass-range 113–147. All the measured yields obtained are new data since *no experimental independent yields* in the fast fission of ^{233}U were available prior to this study.

The yield data were compared with the estimated values from the Z_p semi-empirical model of Wahl and with the calculated values from a new thermodynamical model. A rather good agreement between the experimental data and the calculated/evaluated ones can be observed through the isotopic yield distributions for all investigated elements. In the valley, some noticeable differences between the experimental data and Wahl's estimates can be pointed out. Due to the lack of experimental data in the symmetry region, the empirical model by Wahl shows a high uncertainty in the estimate of the yields in this region. On the other hand, the fission product yields calculated in the new thermodynamical approach show a surprisingly good agreement with the experimental values, in particular in the region of the symmetric fission. This model looks promising and it opens new ways to investigate and model the still enigmatic fission process.

The analysis of the charge distribution shows evidence of the odd-even effect, which has already been observed in the previous studies of the thermal fission of ^{233}U.

A survey of the behavior of the yield distributions *versus* the incident neutron energy became possible by comparison with the previous data for the ^{233}U fission reaction also measured at OSIRIS. This study agrees with previous investigations demonstrating the reduction of the asymmetry in the mass distribution with an increasing energy of the incident neutron. A similar observation was noted in the comparison of the thermal and fast fission of ^{233}U with regards to the charge distribution. Since the systematics in the behavior of the charge yield distribution *versus* excitation energy has not been investigated so far (due to the lack of experimental data), these last results open ways to further studies on different fissioning systems.

A study of the partitioning of the different isomeric state yields was also performed, based on the comparison of yield data from $^{238}\mathrm{U}(\mathrm{n_f}, \mathrm{f})$, $^{235}\mathrm{U}(\mathrm{n_{th}}, \mathrm{f})$ and $^{233}\mathrm{U}(\mathrm{n_f}, \mathrm{f})$ reactions measured at Studsvik. The generally good agreement between the isomeric yield distributions for the three fissioning systems indicates that the relative population of the isomeric states is more closely related to the nuclear properties of the fission products than to the fission process itself.

The authors wish to express their gratitude to the Commissariat à l'Energie Atomique, Department of Nuclear Reactor Physics, and to the Department of Neutron research, Studsvik, for financial support. Deep acknowledgements are expressed to R Håkansson, Reactor Physics Division of Studvik Nuclear AB, W. Gudowski, J. Kierkegaard, and E. Möller, Department of Nuclear and Reactor Physics, Royal Institute of Technology, Stockholm, for the significant help in the flux calculations. We also want to acknowledge the technical staff of the OSIRIS facility for all assistance during the experiment.

References

1. B. Fogelberg, M. Hellström, L. Jacobsson, D. Jerrestam, L. Spanier, G. Rudstam, Nucl. Instrum. Methods Phys. Res. B **70**, 137 (1992).
2. G. Rudstam, Nucl. Instrum. Methods Phys. Res. A **256**, 465 (1987).
3. H. Penttilä, P. Dendooven, A. Honkanen, M. Huhta, P.P. Jauho, A. Jokinen, G. Lhersonneuau, M. Oinonen, J.-M. Parmonen, K. Perijärvi, J. Äysto, Nucl. Instrum. Methods Phys. Res. B **126**, 213 (1997).
4. C. Rubbia, J.A. Rubio, S. Buono, F. Carminati, N. Fiétier, J. Calvez, C. Gelès, Y. Kadi, R. Klapisch, P. Mandrillon, J.P. Revol, Ch. Roche, CERN Report CERN/AT/95-44(ET) (1995).
5. Status report, *Accelerator driven systems: Energy generation and transmutation of nuclear waste*, IAEA-TECDOC-985, (IAEA Vienna, 1997).
6. M. Salvatores, M. Spiro, I. Slessarev, A. Tchistiakov, Y. Terrien, H. Mouney, J. Vergnes, *Role of Accelerator Driven Systems in Waste Incineration Scenarios* presented at *International Conference on Future Nuclear Systems Global'97, Yokohama, Japan. October 5-10*, (JAERI, 1997) p. 561.
7. J. Galy, *Feasibility of the measurement of the fast fission yield of* ^{233}U. *Characterization of the neutron flux produced by the R2-0 reactor*, DEA degree report, INSTN (1996) (Available from the author).
8. W.A. Rhoads, R.L. Childs, *The DORT Two Dimensional Discrete Ordinates Transport Code System, RSIC-CCC-484*, (ORNL Radiation Shielding Information Center, Oak Ridge, TN, 1989).
9. Judith F. Briesmeister, (Editor), *MCNP*$^{\rm TM}$*: A general Monte Carlo N-particle transport method code*, Los Alamos National laboratory report, LA-12625-M (March 1997).
10. L. Jacobsson, B. Fogelberg, B. Ekström, G. Rudstam, Nucl. Instrum. Methods Phys. Res. B **26**, 223 (1987).
11. G. Rudstam, P. Aagaard, B. Ekström, H. Göturk, H.U. Zwicky, Radiochimica Acta **49**, 155 (1990).
12. G. Rudstam, P. Aagard, H.U. Zwicky, Studsvik Science Research Laboratory Report NFL-42, Studsvik, Sweden (1985).
13. G. Rudstam, P.I. Johansson, K. Aleklett, J. Eriksen, *Proceedings of the International Conference on Nucler Data for Science and technology May 9-13, 1994*, (American Nuclear Society, Inc., 1994) p. 977.
14. G. Rudstam, Nucl. Instrum. Methods Phys. Res. A **256**, 465 (1987).
15. J. Galy, B. Fogelberg, F. Storrer, H. Mach, *Yields of long lived fission products produced following* ^{233}U(n_f, f), in preparation.
16. A.C. Wahl, in *New Directions in Physics*, edited by N. Metropolis, (Academic Press, New York, 1987) p. 163.
17. A.C. Wahl, Atomic Data and Nuclear Data Tables **39**, 1 (1988).
18. A.C. Wahl, *Proc. of Specialists Meeting on Fission Product Nuclear Data, Tokai, Japan, May 25-27.* 1992, NEA/NSC, DOC(92), 1992, p. 334.
19. A.C. Wahl, private communication (1998).
20. *Calculations related to nuclear fission-product yields*, Three papers by E. Bogomolova, A. Grashin, A. Efimenko and I. Lukasevich, translated by IAEA, INDC(CCP)-404, IAEA, Vienna (1997).
21. G. Rudstam, *Proceedings of Specialists' Meeting on Fission Product Nuclear Data, Tokai, Japan, 25-27 May, 1992*, NEA/NSC, DOC(92)9 1992, p. 27.
22. J. Galy, *Investigation of the fission yields of the fast neutron-induced fission of* ^{233}U, thesis submitted to the Universitè de Provence Marseille for the degree of Doctor of Philosophy (September 1999).
23. G. Rudstam, INDC(SWD)-024, IAEA, Vienna (1993).
24. R.B. Firestone, *Table of Isotopes*, Eighth Edition, (John Wiley and Sons, Inc., 1996 and update 1998).
25. G. Rudstam, P.I. Johansson, J. Eriksen, Studsvik Science Research Laboratory Report NFL-78, Studsvik, Sweden (1996).
26. R.W. Waldo, R.A. Karam, R.A. Meyer, Phys. Rev. C **23**, 1113 (1981).
27. J. Laurec, A. Adam, T. Debruyne, *Determination of the fission yields of* ^{233}U, ^{235}U, ^{238}U, ^{239}Pu *induced by a spectra of fission neutrons and neutrons of 14.7*MeV (in French), CEA Report CEA-R-5147 (1981).
28. S. Amiel., H. Feldstein, *Proc. of the* 3^{rd} *IAEA Symposium on the Physics and Chemistry of Fission*, Vol. **II** (IAEA, Vienna, 1974), p. 65.
29. A.C. Wahl, J. Radioanal. Chem. **55**, 11 (1980).
30. F. Gönnenwein, Nucl. Instrum. Methods Phys. Res. A **316**, 405 (1992).
31. M. Davi, H.O. Denschlag, H.R. Faust, F. Gönnenwein, S. Oberstedt, I. Tsekhanovitch, M. Wöstheinrich, 2^{nd} *International Workshop on Nucler Fission and Fission-Product Spectroscopy, Seyssins, France*, AIP Conf. Proc. **447**, 239 (1998).
32. U. Quade, K. Rudolph, S. Skorka, Nucl. Phys. A **487**, 1 (1988).
33. F. Gönnenwein, in: C. Wagemans (Editors): *The Nuclear Fission Process*, (CRC Press, Boca Raton, 1991).
34. H. Nifenecker, G. Mariopopoulos, J.P. Bocquet, R. Brissot, J. Cranon, Ch. Ristori, Z. Phys. A **308**, 39 (1982).
35. F. Gönnenwein, J.P. Bocquet, R. Brissot, *Proceedings of the XVII International Symposium Nuclear physics*, (Gaussig, GDR, 1987) p. 129.
36. F. Gönnenwein, *Proceedings of the XVIII International Symposium Nuclear Physics*, (Gaussig, GDR, 1988), Rossendorf report zfk-646 (1988) p. 129.
37. D.G. Madland, T.R. England, Nucl. Sci. Eng. **64**, 859 (1977).
38. G. Rudstam, *Proceedings of International Conference on Nuclear Data for Scince and Technology, May 9-13, 1994*, (American Nuclear Society, Inc., 1994) p. 955.
39. K.-H. Schmidt, A. Heinz, H.-G. Clerc, B. Blank, T. Brohm, S. Czajkowski, C. Donzaud, H. Geissel, E. Hanelt, H. Irnich, M.C. Itkis, M.de Jong, A. Junghans, A. Magel, G. Muenzenberg, F. Nickel, M. Pfuetzner, A. Piechaczek, C. Roehl,

C. Scheidenberger, W. Schwab, S. Steinhaeuser, K. Suemmerer, W. Trinder, B. Voss, S.V. Zhdanov, Phys. Lett. B **325**, 313 (1994).
40. T.R. England, B.F Rider, ENDF-349, Los Alamos National Laboratory, LA-UR-94-3106 (1994).
41. U. Brosa, S. Gro mann, A. Müller, Phys. Rep. **197**, 167 (1990).
42. K.-H. Schmidt, S. Steinhäuser, C. Böckstiegel, A. Grewe, J. Benlliure, H.-G. Clerc, A. Heinz, M.de Jong, A.R. Junghans, J. Müller, M. Pfützner, 2^{nd} *International Workshop on Nucler Fission and Fission-Product Spectroscopy, Seyssins, France*, AIP Conf. Proc. **447**, 407 (1998).
43. Tie-shuan fan, Ji-min Hu, Shang-lian Bao, Nucl. Phys. A **591**, 161 (1995).
44. K. Kobayashi, Z. Li, Y. Fujita, *Proceedings of Specialists' Meeting on Fission Product Nuclear Data, Toakai, Japan 25-27 May 1992*, (NEA/NSC, DOC(92)9, 1992) p. 299.
45. F. Vivès, *Investigation of the fission fragment properties of the reaction* $^{238}\mathrm{U(n,f)}$ *at the incident neutron energy up to 5.8*MeV, thesis sumitted to the University of Bordeaux I for the degree of Doctor of Philosophy, November 1998.